# Interaction of Fast Neutrons with Oriented $Ho^{165}$†

T. R. FISHER, R. S. SAFRATA,* E. G. SHELLEY,‡ J. MCCARTHY, AND S. M. AUSTIN,§‖
*Department of Physics, Stanford University, Stanford, California*

AND

R. C. BARRETT
*Lawrence Radiation Laboratory, University of California, Berkeley, California*

(Received 28 November 1966)

Total cross-section and angular distribution measurements are reported for 8- and 15-MeV neutrons incident on unoriented $Ho^{165}$. Measurements of the "deformation effect" in the total cross section for unpolarized neutrons incident on oriented $Ho^{165}$ at 8 and 15 MeV are also reported. The first and second moments of the nuclear orientation were $B_1/B_1(\max)=+0.55$ and $B_2/B_2(\max)=+0.25$. If the "deformation effect" is defined by $\Delta\sigma_{\mathrm{Def}}=\sigma(\text{oriented})-\sigma(\text{unoriented})$, the experimental results for $\Delta\sigma_{\mathrm{Def}}$ are $-38\pm10$ mb and $-139\pm16$ mb at 8 and 15 MeV, respectively. The above data are explained by a coupled-channel analysis based on the rotational optical model, and the optical parameters derived from this analysis are used to interpret a measurement of the "spin-spin effect" at $E_n=7.85$ MeV. The neutron polarization for the measurement was 0.34. If the "spin-spin effect" is defined by $\Delta\sigma_{ss}=\sigma_{\uparrow\uparrow}-\sigma_{\uparrow\downarrow}$, the experimental result for $\Delta\sigma_{ss}$ is $+3\pm13$ mb at $E_n=7.85$ MeV. If $\Delta\sigma_{ss}$ is assumed to arise from a term of the form $-V_{ss}f(r,r_0A^{1/3},a)\times\mathbf{I}\cdot\sigma/I$ in the optical potential, the acceptable limits on the strength of the potential are $-340$ keV $<V_{ss}<540$ keV. The present experimental results are compared with other published data on the interaction of neutrons with oriented $Ho^{165}$.

## I. INTRODUCTION

A NUMBER of investigations, both experimental and theoretical, have been reported on the interaction of fast neutrons and protons with oriented heavy nuclei. These investigations may be divided into two general categories: the interaction of unpolarized nucleons with oriented, deformed nuclei; and the interaction of polarized nucleons with polarized nuclei. From investigations in the first category, one hopes to gain direct evidence on the sign and magnitude of the nuclear deformation; investigations in the second category provide information on the spin-spin interaction between a nucleon and a heavy nucleus. Three approaches, based on a deformed potential well model, have been applied to the theoretical calculations: the black-nucleus approximation, distorted-wave Born approximation (DWBA), and the coupled-channel formalism. The experimental investigations have been confined to the particular nucleus $Ho^{165}$. This nucleus has a large quadrupole deformation (the accepted value for $\beta$ is 0.3)[1–4] and is therefore well suited to a study of effects arising from nuclear deformation. With present experimental techniques, large nuclear polarizations (>50%) have been obtained in holmium samples as large as one mole. The experimental work discussed in this paper involves measurements of the total cross section for unpolarized and polarized neutrons incident on oriented $Ho^{165}$ nuclei.

The formalism for the black-nucleus approximation has been presented by Visotskii *et al.*[5] Davies *et al.*,[6] using the DWBA, have calculated cross sections for the elastic scattering of unpolarized neutrons and protons by oriented $Mn^{55}$ and $Ho^{165}$ nuclei. A coupled-channel calculation on the elastic scattering of unpolarized neutrons of energy $E_n=1$ MeV by oriented $Ho^{165}$ nuclei has been reported by Barrett.[7] The calculations in Refs. 5, 6, and 7 predicted that the cross sections for the scattering of nucleons by deformed nuclei would depend strongly on the nuclear orientation. The effect of nuclear deformation on the total cross section for neutrons incident on oriented $Ho^{165}$ nuclei has since been observed at $E_n=0.350$ MeV by Wagner *et al.*,[8] and at $E_n=14$ MeV by Marshak *et al.*[9] Preliminary results of similar work at $E_n=8$ and 15 MeV have been presented by the authors.[10] In Refs. 8 and 9 the experimental results are successfully explained by an analysis based on the coupled-channel formalism. A comprehensive review of this formalism has been given by Tamura.[11] The change in total cross section resulting

† This work was supported in part by the Office of Naval Research, the National Science Foundation, and the U. S. Atomic Energy Commission.

* Present address: Nuclear Research Institute, Rez, Czechoslovakia.
‡ Recipient of Lockheed Independent Research Funds.
§ Present address: Department of Physics, Michigan State University, East Lansing, Michigan.
‖ Sloan Foundation Fellow.

[1] M. Danos and W. Greiner, Phys. Letters **8**, 114 (1964).
[2] B. Elbek, *Determination of Nuclear Transition Probabilities by Coulomb Excitation* (Ejnar Munksgaard, Copenhagen, 1963).
[3] E. Ambler, E. G. Fuller, and H. Marshak, Phys. Rev. **138**, B117 (1965).
[4] S. A. DeWit, G. Backenstoss, C. Daum, and J. C. Sems (to be published).
[5] G. L. Vysotskii, E. V. Inopin, and A. A. Kresnin, Zh. Eksperim. i Teor. Fiz **36**, 574 (1959) [English transl.: Soviet Phys.—JETP **9**, 398 (1959)].
[6] K. T. R. Davies, G. R. Satchler, R. M. Drisko, and R. H. Bassel, Nucl. Phys. 44, 607 (1963).
[7] R. C. Barrett, Nucl. Phys. **51**, 27 (1964).
[8] R. Wagner, P. D. Miller, T. Tamura, and H. Marshak, Phys. Rev. **139**, B29 (1965).
[9] H. Marshak, A. C. B. Richardson, and T. Tamura, Phys. Rev. **150**, 996 (1966).
[10] E. G. Shelley, T. R. Fisher, R. S. Safrata, J. McCarthy, and S. M. Austin, Phys. Letters **19**, 684 (1966).
[11] T. Tamura, Rev. Mod. Phys. **37**, 679 (1965).

from nuclear orientation when neutrons are incident on a deformed nucleus will frequently be referred to as the "deformation effect." It may be defined by $\Delta\sigma_{\mathrm{Def}} = \sigma(\text{oriented}) - \sigma(\text{unoriented})$, where $\sigma$(oriented) and $\sigma$(unoriented) are the total cross sections for the oriented and unoriented cases.

The inclusion of a spin-spin term of the form[12] $-V_{ss}f(r,r_0A^{1/3},a)\mathbf{I}\cdot\boldsymbol{\sigma}/I$ in the optical potential was first suggested by Feshbach.[13] Khan[14] has considered the possibility that such a term may be responsible for a systematic difference in neutron $s$-wave strength functions for even- and odd-$A$ nuclei in the mass region around $A=65$. Davies and Satchler,[15] using the DWBA, have calculated the effects of such a term on the elastic scattering of polarized neutrons by polarized $Mn^{55}$ and $Ho^{165}$ nuclei. The results of Bloom *et al.*[16] indicate that the residual interaction between two nucleons bound in a potential exhibits a large spin dependence similar to that in the free nucleon-nucleon interaction. Estimates of the magnitude of $V_{ss}$, based on the spin dependence of the free nucleon-nucleon interaction, are of the order of 50–100 keV.[14,17] This prediction is in agreement with the conclusion of Rosen *et al.*[18] that $V_{ss}$ is small compared with the terms usually included in the optical potential.

An attempt to observe directly the effect due to a spin-spin term in the optical potential has been made by Wagner *et al.*[8] In their experiment, polarized neutrons of energy 0.350 MeV were incident on a polarized $Ho^{165}$ target and the total cross section was measured as a function of the relative spin orientation. Preliminary results of a similar experiment performed at $E_n=7.85$ MeV have been presented by the authors.[17] The change in total cross section resulting from a change in the relative spin orientation when polarized neutrons are incident on a polarized target will frequently be referred to as the "spin-spin effect." It may be defined by $\Delta\sigma_{ss} = \sigma_{\uparrow\uparrow} - \sigma_{\uparrow\downarrow}$, where $\sigma_{\uparrow\uparrow}$ and $\sigma_{\uparrow\downarrow}$ are the total cross sections for the parallel and antiparallel spin configurations.

In the present paper, a more complete description of experimental results reported by the authors in Refs. 10 and 17 is presented together with an extensive theoretical investigation of both the deformation and spin-spin effects. The coupled-channel formalism in adiabatic approximation is used in the analysis.[7,11] In addition to the experiments with oriented $Ho^{165}$ nuclei, measurements of the differential elastic and total cross sections performed with unpolarized neutrons and an unoriented $Ho^{165}$ target are described. These measurements are required to establish the optical parameters describing the interaction of fast neutrons with $Ho^{165}$.

In Sec. II, the technique for producing nuclear orientation is discussed with particular emphasis on the determination of the nuclear orientation parameters for our sample of polycrystalline holmium metal. In Sec. III, the main pieces of experimental apparatus are described. Section IV describes the various phases of the experimental work and the theoretical analysis of the experimental results is presented in Sec. V. A complete description of the coupled-channel formalism in adiabatic approximation is omitted, since this can be found elsewhere.[7,11] However, systematics of the deformation and spin-spin effects as a function of neutron energy are presented and the dependence of $\Delta\sigma_{\mathrm{Def}}$ and $\Delta\sigma_{ss}$ on the choice of optical parameters is investigated. In Sec. VI, some general conclusions are presented and areas for further experimental work are suggested.

## II. DETERMINATION OF NUCLEAR ORIENTATION PARAMETERS FOR THE POLYCRYSTALLINE HOLIUM SAMPLE

The large hyperfine splitting[19–22] in $Ho^{165}$ and the ferromagnetic state of the metal at low temperatures[23] make it possible to achieve substantial nuclear orientation by cooling the metal below 1°K in a magnetic field of few kOe. This technique is referred to as the ferromagnetic method.[24] The hyperfine field in holmium metal is of the order of 8 MOe. This field removes the degeneracy of the nuclear magnetic substates, and significant asymmetry in the population of these substates occurs at temperatures $<1$°K. At low temperatures, an external field of a few kOe is sufficient to magnetically saturate a holmium single crystal. The $z$ axis of quantization for the nuclear spin system then coincides with the direction of the applied field. A good discussion of this technique as applied to a holmium single crystal is given in Ref. 8. Our discussion will deal mainly with the problem of the determination of orientation parameters when the holmium metal is polycrystalline.

The most fundamental description of a system of nuclear spins is provided by the density matrix $\rho_{MM'}$. In many cases, it is more convenient to work with an

---

[12] $V_{ss}$ is usually called the "strength" of the spin-spin potential, and $f(r,r_0A^{1/3},a)$ is a form factor which is usually taken to have a Woods-Saxon shape. The spin-spin potential is also written $-V_{ss}f(r,r_0A^{1/3},a)\mathbf{I}\cdot\boldsymbol{\sigma}$ and $-V_{ss}f(r,r_0A^{1/3},a)\mathbf{I}\cdot\mathbf{s}$. The "strength" $V_{ss}$ depends on the particular form chosen since $(\mathbf{I}\cdot\boldsymbol{\sigma}/I)=(2/7)\mathbf{I}\cdot\boldsymbol{\sigma}=(4/7)\mathbf{I}\cdot\mathbf{s}$ in the case of $Ho^{165}$.

[13] H. Feshbach, *Nuclear Spectroscopy*, edited by F. Ajzenberg-Selove (Academic Press Inc., New York, 1960), Part B, p. 1046.

[14] M. Z. Rahman Kahn, Nucl. Phys. **76**, 475 (1966).

[15] K. T. R. Davies and G. R. Satchler, Nucl. Phys. **53**, 1 (1964).

[16] S. D. Bloom, J. D. Anderson, W. F. Hornyak, and C. Wong, Phys. Rev. Letters **15**, 364 (1965).

[17] T. R. Fisher, E. G. Shelley, R. S. Safrata, J. McCarthy, and R. C. Barrett, Phys. Rev. Letters **17**, 36 (1966).

[18] L. Rosen, J. E. Brolley, Jr., and L. Stewart, Phys. Rev. **121**, 1423 (1961).

[19] B. Bleaney, J. Phys. Soc. (Japan) **17**, Suppl. B-1, 435 (1962).

[20] O. V. Lounasama, Phys. Rev. **128**, 1136 (1962).

[21] H. Van Kempen, A. R. Miedema, and W. J. Huiskamp, Physica **30**, 229 (1964).

[22] G. Brunhart, H. Postma, and V. L. Sailor, Phys. Rev. **137**, B1484 (1965).

[23] B. L. Rhodes, S. Legvold, and F. H. Spedding, Phys. Rev. **109**, 1544 (1958).

[24] G. R. Khutsishvili, Zh. Eksperim. i Teor. Fiz. **29**, 894 (1955) [English transl.: Soviet Phys.—JETP **2**, 744 (1956)].

alternative description in terms of the statistical tensors[25]

$$B_{KQ}=(2I+1)^{1/2}\sum_{M,M'}\rho_{MM'}(-)^{K-I-M}(KQ|II-MM'),$$
$$0\leq K\leq 2I,\ -K\leq Q\leq K. \quad (1)$$

The quantities $B_{KQ}$ transform like the components of irreducible spherical tensors under rotations of the coordinate axes. If the spin system has axial symmetry, $\rho_{MM'}=P_M\delta_{MM'}$ where the $P_M$'s denote the population densities of the nuclear magnetic substates, and $B_{KQ}=B_K\delta_{Q0}$. We will restrict our discussion to systems with axial symmetry, so that the degree of nuclear orientation is completely specified by the set of parameters $P_M$ or $B_K$.

Taking the direction of the applied field as the $z$ axis, we now give expressions for the nuclear orientation parameters in magnetically saturated holmium metal. The hyperfine interaction is described by the Hamiltonian[19]

$$\mathcal{H}=-a'I_z+P[I_z^2-\tfrac{1}{3}I(I+1)]. \quad (2)$$

The nuclear spin is $I$ and its projection $I_z$. The quantities $a'$ and $P$, the strengths of the dipole and quadrupole interactions respectively, are known from specific heat measurements and measurements on the transmission of polarized thermal neutrons[22] through polarized $Ho^{165}$. The dipole term $a'I_z$ is dominant; thus, since $a'>0$, the lowest energy state for $Ho^{165}$ has $I_z=+\frac{7}{2}$. An average of the most recent specific heat measurements[20,21] leads to the values $a'=(0.320\pm0.005)°K$ and $P=0.007\pm0.0015°K$.[26] The population densities $P_M$ of the nuclear magnetic substates as a function of temperature $T$ are derived from the Boltzman distribution

$$P_M=\exp(-E_M/kT)/[\sum_{M'}\exp(-E_{M'}/kT)],$$
$$E_M=-kMa'+kP[M^2-\tfrac{1}{3}I(I+1)]. \quad (3)$$

If the holmium metal is not magnetically saturated, but the atomic moments have some probability distribution $W(\theta)d\theta$ which is symmetric with respect to the direction of the external field, the following expressions for the statistical tensors may be derived

$$B_K=B_K(T)\langle P_K(\cos\theta)\rangle,$$
$$B_K(T)=(2I+1)^{1/2}\sum_M P_M(-)^{K-I-M}(K0|II-MM),$$
$$\langle P_K(\cos\theta)\rangle=\int_0^\pi P_K(\cos\theta)W(\theta)d\theta\Big/\int_0^\pi W(\theta)d\theta, \quad (4)$$

where $P_K(\cos\theta)$ is the Legendre polynomial of order $K$, and $P_M$ is given by Eq. (3). For the special case of magnetic saturation, $W(\theta)=\delta(\theta)$, $\langle P_K(\cos\theta)\rangle=1$ and $B_K=B_K(T)$.

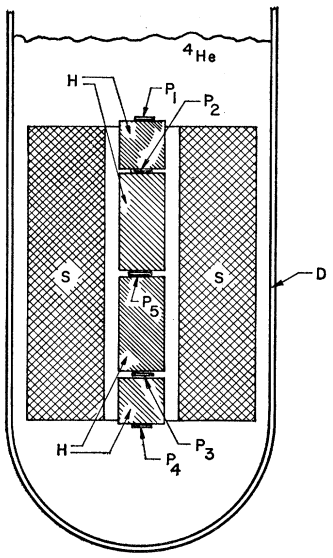


FIG. 1. Experimental arrangement for magnetization measurements. $H$, holmium cylinders; $S$, superconducting solenoid; $D$, $He^4$ Dewar; $P$, Hall probe. The numbers 1–5 indicate points for the placement of Hall probes as described in Sec. II.

The holmium sample used in the experimental work with oriented $Ho^{165}$ nuclei was a cylinder of polycrystalline metal, 1.6 cm diam×10.9 cm long,[27] composed of four shorter cylindrical sections.[28] The external magnetic field was applied parallel to the axis of the cylinder but was insufficient to saturate the polycrystalline metal. Magnetization data were therefore required for the determination of the nuclear orientation parameters, and these were obtained in a separate measurement performed at a temperature of 4.2°K.

The experimental set-up for the magnetization measurements is shown in Fig. 1. From the $B$ field, measured by the Hall probe[29] $P_5$ in the figure, one obtains a magnetization curve characteristic of the metal in the vicinity of the probe. The expressions relating $B$, $M$, and $H_0$, where $H_0$ is the field at the center of the solenoid, are given in Appendix I. By rearranging the order of the four cylindrical sections, magnetization curves typical of different regions in the sample were obtained. These showed no significant variations, and the magnetization curve characteristic of the sample is shown in Fig. 2.

The average magnetization of the sample at the solenoid field used in the experiments with oriented

[25] Many definitions of the statistical tensors have been given. The definition used here is that of Ref. 6.

[26] In Refs. 8 and 9, a slightly different value (0.310) for $a'$ is chosen and $P$ is neglected. The differences in the orientation parameters due to these changes are very small and do not affect the comparison between our results and those of Refs. 8 and 9.

[27] The holmium metal was obtained from Lunex Company, Pleasant Valley, Iowa. The purity was 99.9% (manufacturer's quotation). The value 11.1 cm, which is quoted as the length of the holmium sample in Ref. 10, is slightly in error.

[28] The use of a long sample with low transmission (the transmission of our sample was about 0.18) enhances the experimental sensitivity for the detection of a small change in the total cross section. Since large single crystals of holmium are not available, the choice lies between a large polycrystalline sample or a much smaller single crystal. Each alternative has certain advantages and disadvantages. The choice here was made in favor of a long polycrystalline cylinder, and it was then most natural to choose the $z$ axis for the nuclear orientation parallel to the axis of the cylinder and the direction of the neutron beam.

[29] Hallefex thin-film Hall Generator, Beckman Instruments, Inc.

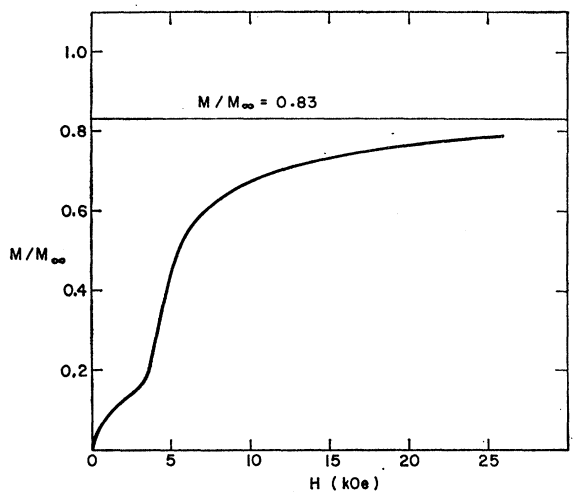


FIG. 2. Magnetization curve for polycrystalline holmium sample used in the experiments with oriented $Ho^{165}$ nuclei. Since the curve was recorded with an $x$-$y$ recorder, individual points are not shown. The 83% plateau, which is predicted by the model for an ideal polycrystal, is indicated in the figure.

$Ho^{165}$ nuclei was measured by inserting four additional Hall probes, $P_1$ through $P_4$, in Fig. 1. Equation (A1), Appendix I, was not used to relate the readings of probes $P_1$ through $P_4$ to the magnetization at these points since the demagnetizing factor $N$ could not be estimated accurately. It will be observed, however, that the curve of Fig. 2 may be used to relate $B$ to $M$ at the points corresponding to the position of probes $P_1$ through $P_4$. The magnetization was plotted as a function of distance along the axis of the cylinder, and this curve was integrated to give the average magnetization. The result[30] was $M/M_\infty=0.70\pm0.03$, where $M_\infty=350$ cgs units/g, the saturation magnetization for holmium. This average magnetization was produced by a field of[18] kOe at the center of the solenoid,[30] the field which could safely be used when the solenoid was operated in vacuum.

The quantity $\langle P_1(\cos\theta)\rangle$ is directly related to the average magnetization: $\langle P_1(\cos\theta)\rangle=M/M_\infty$. The values of $\langle P_K(\cos\theta)\rangle$ for $K>1$ are not uniquely determined by the magnetization measurement, but may be obtained from a reasonable model. A model based on the following assumptions was adopted: (1) The polycrystalline metal can be described as a large collection of randomly oriented single crystals; (2) under the application of an external field, each single crystal exhibits the behavior which would be predicted from single-crystal magnetization curves. A similar model for polycrystalline holmium is discussed by Miwa and Yosida.[31] The magnetization curve for such an idealized polycrystal is expected to show an inflection point in the low field region and a plateau at about 83% of saturation magnetization. These qualitative features are exhibited in the curve of Fig. 2, and their explanation is discussed in Ref. 32. Thus, an idealized polycrystal becomes effectively "saturated" in moderate fields at a magnetization $M/M_\infty=0.83$. Under these conditions the quantities $\langle P_K(\cos\theta)\rangle$, which will be denoted by $\langle P_K(\cos\theta)\rangle_{\rm sat}$, are given by

$$\langle P_K(\cos\theta)\rangle_{\rm sat}=(6/\pi)\int_0^{\pi/2}d\theta'\int_0^{\pi/6}d\Phi'\,\sin\theta' P_K(\cos\beta)\,, \tag{5}$$

$$\cos\beta=\cos\theta'\cos\theta_0+\sin\theta'\sin\theta_0\cos\Phi',\quad \theta_0=80°.$$

Equation (5) is a generalization of Eq. (4.8) of Ref. 31. Since in our actual sample $M/M_\infty$ was 0.70 rather than 0.83, it was assumed that for our sample $\langle P_K(\cos\theta)\rangle=(0.70/0.83)\langle P_K(\cos\theta)\rangle_{\rm sat}$, where $\langle P_K(\cos\theta)\rangle_{\rm sat}$ is given by Eq. (5). Several alternatives to this last assumption were also considered; the results were used to estimate uncertainties for the quantities $\langle P_K(\cos\theta)\rangle$ for $K>1$.

TABLE I. Nuclear orientation parameters $B_K$ for polycrystalline holmium sample at 0.34°K and $M/M_\infty=0.70$.

| $K$ | $B_K(T)$ | $\langle P_K(\cos\theta)\rangle$ | $B_K$ | $B_K/B_K(\max)$ |
|---|---|---|---|---|
| 0 | 1 | 1 | 1 | 1 |
| 1 | 1.21 | 0.70 | 0.84 | 0.55±0.03 |
| 2 | 0.79 | 0.48 | 0.38 | 0.25±0.05 |
| 3 | 0.34 | 0.28 | 0.096 | 0.06±0.02 |
| 4 | 0.10 | 0.15 | 0.015 | 0.02±0.01 |

In Table I, the quantities $B_K(T)$, $\langle P_K(\cos\theta)\rangle$, $B_K$, and $B_K/B_K(\max)$ are tabulated[33] for $K\leq4$. These values correspond to a temperature of 0.34°K. The values of $B_K$ for $K>4$ are negligibly small. The uncertainties in the values of $B_K(T)$ are due to uncertainties in $a'$, $P$, and $T$ and are negligible in comparison with uncertainties in the quantities $\langle P_K(\cos\theta)\rangle$. The large uncertainties allowed for $\langle P_K(\cos\theta)\rangle$ and consequently for $B_K/B_K(\max)$ with $K>1$ are due to the dependence of these quantities on the particular model chosen. However, these errors were obtained from a consideration of rather extreme cases, and should be regarded more as limits on the uncertainty rather than as prob-

[30] In Ref. 10, the value $M/M_\infty=0.62\pm0.03$ is quoted and the solenoid field is given as 22 kOe. Actually, the solenoid field was first increased to 22 kOe and then reduced to 18 kOe. The reduction in field afforded safer operation in the persistent current mode, and caused no significant loss in magnetization due to the hysteresis of the holmium metal. The change in $M/M_\infty$ from 0.62 to 0.70 comes about as follows. In Ref. 10, no correction was made for the demagnetizing field of the gap which accommodated the Hall probe. This raises the value of $M/M_\infty$ to 0.66. This result was averaged with additional data to obtain the result $M/M_\infty=0.70$ which is quoted here.

[31] Hirosi Miwa and Kei Yosida, Progr. Theoret. Phys. (Kyoto) **26**, 693 (1961).

[32] R. S. Safrata, T. R. Fisher, and E. G. Shelley, J. Appl. Phys. **37**, 4869 (1966).

[33] The orientation parameters given in Refs. 10 and 17 were computed assuming $M/M_\infty=0.62$ and $P=0$ in Eq. 2. The final parameters adopted here were computed from $M/M_\infty=0.70$ and $P=0.007$. The increase in magnetization is accidentally compensated by the inclusion of the quadrupole term $P$ in Eq. 2, so that the final parameters differ very little from those quoted in Refs. 10 and 17.

TABLE II. Population densities of nuclear magnetic substates for polycrystalline holmium sample at 0.34°K, $M/M_\infty=0.70$.

| $M$ | $-\frac{7}{2}$ | $-\frac{5}{2}$ | $-\frac{3}{2}$ | $-\frac{1}{2}$ | $+\frac{1}{2}$ | $+\frac{3}{2}$ | $+\frac{5}{2}$ | $+\frac{7}{2}$ |
|---|---|---|---|---|---|---|---|---|
| $P_M$ | 0.023 | 0.028 | 0.039 | 0.058 | 0.092 | 0.148 | 0.237 | 0.375 |

able errors or standard deviations. The population densities ($P_M$) are given in Table II; these were obtained from the $B_K$'s in Table I by inverting the set of Eqs. (1).

## III. EXPERIMENTAL APPARATUS

### A. Experiments with Unoriented Nuclei

The reactions $Be^9(\alpha,n)C^{12}$ and $H^3(d,n)He^4$ were used to produce neutrons of energies $E_n=8$ and 15 MeV, respectively. The Stanford 3-MV electrostatic accelerator furnished a source of 2.65-MeV $\alpha$ particles and 250-keV deuterons. The particle beams were magnetically analyzed in a uniform field magnet and focused on the target with the aid of an electrostatic quadrupole lens. The analyzing magnet was calibrated from $p$-$n$ threshold measurements using the reactions $Be^9(p,n)B^9$ and $H^3(p,n)He^3$. A defining aperture located 25 cm from the target confined the beam to a circle of 3.2 mm diam. The targets were gyrated and cooled by a stream of air to increase their lifetimes. Targets of $Be^9$ averaging 400 $\mu g/cm^2$ in thickness were prepared by vacuum evaporation onto previously out-gassed tungsten blanks. The technique of electron bombardment was found to be far superior to other methods of evaporation. Targets of titanium impregnated with tritium were commercially obtained.[34]

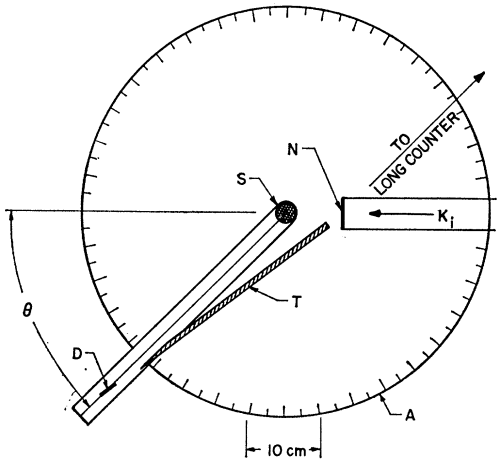


FIG. 3. Experimental arrangement for angular distribution measurements. $A$, light-weight aluminum table; $K_i$, direction of incident particle beam; $N$, target for neutron production; $S$, holmium scatterer; $D$, 200 $mm^2\times2$ mm Si(Li) detector; $T$, tungsten shadow shield. $\theta$ is the scattering angle as measured from the center of the scatterer to the center of the detector. A top view only is shown. The scatterer, detector, and tungsten shield were supported by thin-walled stainless steel tubes at a distance of 25 cm above the top of the aluminum table, $A$. The distance from the source to the center of the scatterer was 7.65 cm, and the distance from the scatterer to the detector was 25 cm and 33 cm for the 8- and 15-MeV measurements, respectively.

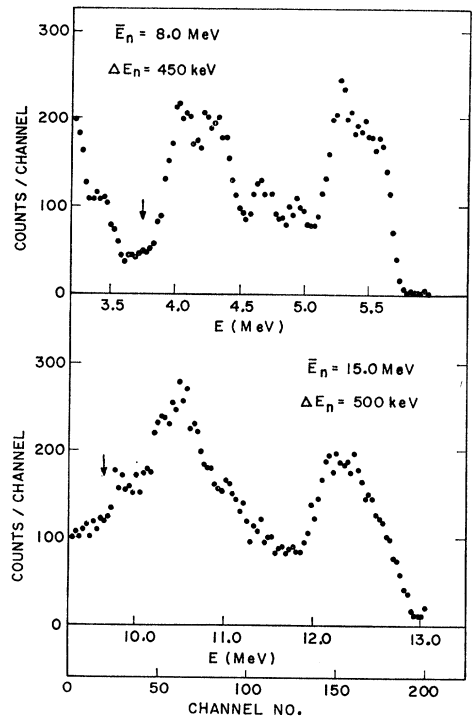


FIG. 4. Spectra from Si(Li) detector at $E_n=8$ and 15 MeV. The spread in the peaks is due to the energy spread in the neutron beam rather than intrinsic detector resolution. The spectra were taken using a biased amplifier, and the suppressed zero on the energy scale should be noted. The energy scale refers not to neutron energy, but to the energy released in the detector by a particular neutron-induced reaction.

Figure 3 shows the experimental arrangement for the differential elastic-cross-section measurements. These measurements were made in open geometry, and a 200 $mm^2\times2$ mm Si(Li) detector was used as the neutron detector. The spectra produced by fast neutrons in such detectors have been described.[35,36] Typical neutron spectra at 8 and 15 MeV are shown in Fig. 4. The neutron source intensity was monitored with the aid of a standard long counter. The Si(Li) detector and the holmium sample were mounted on the light-weight aluminum table shown in Fig. 3, which was aligned with the aid of a transit. The neutron detector was shielded from the direct neutrons by tungsten bars.

### B. Experiments with Oriented $Ho^{165}$ Nuclei

For the experiments involving oriented $Ho^{165}$ nuclei, the key piece of apparatus was the $He^3$ cryostat required for producing nuclear orientation in the holmium sample. The cryostat and associated apparatus will be

[34] U. S. Radium Corporation, Morristown, New Jersey.
[35] L. Colli, I. Iori, M. G. Marcazzan, and M. Milazzo, Nucl. Phys. **43**, 529 (1963).
[36] G. Andersson-Lindstrom and E. Rosele, Phys. Letters **5**, 71 (1963).

referred to as the SCONT system (Stanford cryostat for oriented nuclear targets). Figure 5 shows schematically the general features of the SCONT system. The liquid nitrogen bath and liquid $He^4$ 4.2°K bath occupy a common vacuum space. The pumped $He^4$ 1.2°K bath, the $He^3$ chamber, and the working volume occupy a second common vacuum space. The working volume, which contains the superconducting solenoid and the holmium sample, has the shape of a vertical cylinder of 20 cm diam×23 cm high and is surrounded by a thermal shield at 4.2°K. The outer vacuum jacket, the 77°K thermal shield, and the 4.2°K thermal shield are furnished with thin windows along the beam line, so that the neutron beam passes through a total thickness of 225-$\mu$ aluminum and 25-$\mu$ Mylar in traversing the apparatus. The thin windows were included as a design feature primarily to make possible electron scattering experiments.

Figure 6 shows in more detail the working volume, including the $He^3$ chamber, the superconducting solenoid, the holmium sample, and various monitors. The $He^3$ chamber had a volume of 4 cc and contained a thin copper ribbon wound in the form of a spiral. The spiral was soldered to the base of the chamber and provided

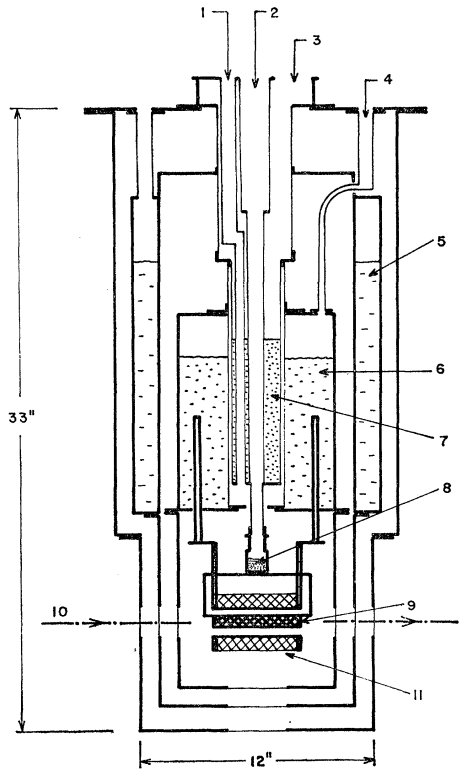


FIG. 5. Schematic drawing of $He^3$ cryostat. 1, pumping line for inner vacuum; 2, pumping line for $He^3$; 3, pumping line for $He^4$ 1.2°K bath; 4, filling line for $He^4$ 4.2°K bath; 5, liquid nitrogen bath; 6, liquid $He^4$ 4.2°K bath; 7, liquid $He^4$ 1.2°K bath; 8, chamber for liquid $He^3$; 9, holmium sample; 10, neutron beam direction (note thin windows along beam line); 11, superconducting solenoid.

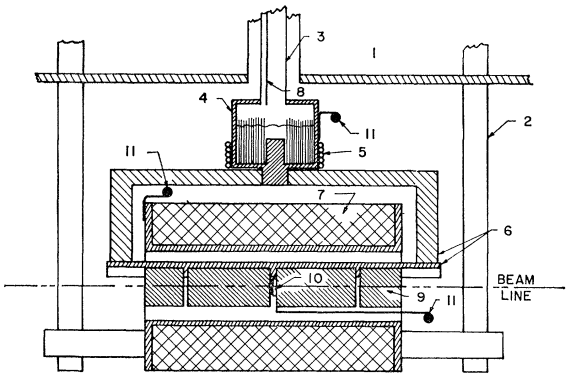


FIG. 6. Interior of $He^3$ cryostat. 1, $He^4$ 4.2°K bath; 2, copper support rods for superconducting solenoid; 3, thin-walled stainless steel tube; 4, $He^3$ chamber; 5, heating coil; 6, thermal link between holmium sample and $He^3$ chamber; 7, superconducting solenoid; 8, $He^3$ return line; 9, holmium sample; 10, Hall probe magnetization monitor; 11, carbon resistor thermometers.

an area of 100 $cm^2$ for heat transfer between the chamber and the liquid $He^3$. The chamber was provided with a heating coil for rapid warming of the sample. The superconducting solenoid, which had dimensions of 8.9 cm length, 3.17 cm i.d., and 7.6 cm o.d., was mounted in vacuum and cooled by its copper support rods which projected into the $He^4$ 4.2°K bath. The solenoid could be operated continuously in vacuum at a central field of 18 kOe; it was normally operated in the persistent current mode, and no significant decay was observed over periods up to 100 hours. The cryostat required approximately 25 liters of liquid $He^4$ for initial cooling; the consumption rate thereafter was approximately 20 liters per day.

Considerable effort was expended to insure good thermal contact between the holmium sample and the $He^3$ chamber. The four cylindrical sections comprising the sample (see Fig. 6) were first soldered[37] into a half-cylindrical section of copper tubing; this was attached to the $He^3$ chamber by copper links with all connections soldered. With this arrangement, the time required to cool the sample from 4.2 to 0.34°K was less than two hours.

The magnetization and temperature of the holmium sample were continuously monitored. The magnetization monitor was a Hall probe[29] placed between the two central cylindrical sections (Fig. 6). Speer carbon resistors (grade 1002, 220Ω, $\frac{1}{2}$ W) were used as temperature monitors. The use of these resistors for temperature measurements in the region 4.2 to 0.3°K has been described.[38] The estimated uncertainty in temperature measurements with the resistors was less than ±0.010°K.

[37] The holmium metal was soldered to the copper using Indalloy #2 solder (Indium Corporation of America) without flux. The solder was applied with a stiff wire brush.

[38] W. C. Black, Jr., W. R. Roach, and J. C. Wheatley, Rev. Sci. Instr. **35**, 587 (1964).

Figure 7 shows the experimental arrangement for the measurement of the deformation effect. Due to the large size of the holmium sample and the complexities inherent in the SCONT system, no attempt was made to move the sample frequently in and out of the beam as is the usual procedure in a neutron transmission experiment. Since the transmission of the sample could be calculated from total-cross-section measurements made in open geometry, however, it was not necessary to measure the actual transmission with the experimental set-up of Fig. 7. If $R$ denotes the ratio of counts recorded by detector $D_2$ to counts recorded by detector $D_1$, where the positions of detectors $D_1$ and $D_2$ are shown in Fig. 7, then $R$ is directly proportional to the transmission of the holmium sample (except for corrections for background and inscattering). A comparison between the value of $R$ when the sample temperature is 0.34°K and the value when the sample temperature is 4.2°K (negligible nuclear alignment) thus gives a measurement of the deformation effect. Because of the long period of time required to cool the sample from 4.2 to 0.34°K it was necessary to make the ratio $R$ extremely stable against all other perturbations affecting the system.

Since the intrinsic energy dependence of the efficiency of the Si(Li) detectors $D_1$ and $D_2$ in Fig. 7 is the same, the ratio $R$ is stable against changes in the intensity and energy distribution of neutrons from the source. To stabilize the ratio against drifts in electronics components, the system illustrated in Fig. 8 was devised. The signals from detectors $D_1$ and $D_2$ were fed through separate low noise preamplifiers. After preamplification the pulses were handled by common electronics and sorted by means of logic pulses furnished by the two preamplifiers. When the gains of the two preamplifiers were properly adjusted, the spectra from detectors $D_1$ and $D_2$ were nearly identical in shape. Thus, only a change in the relative gain of the two preamplifiers could affect the ratio $R$, and the analyzer spectra could be used to estimate a correction for any such observed change. The analyzer and the scalers in Fig. 8 provided

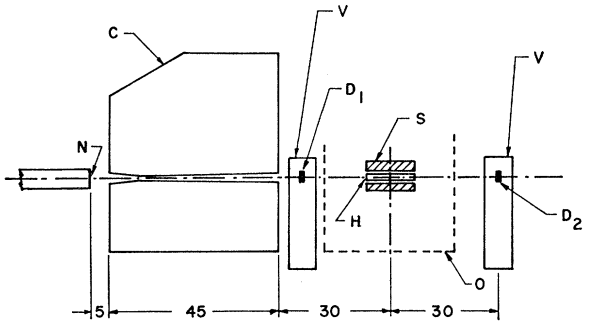


FIG. 7. Experimental arrangement for measurement of the deformation effect. $N$, neutron source; $C$, copper shield; $D_1$, 80 mm² ×2 mm Si(Li) detector; $D_2$, stack of two 200 mm²×2 mm Si(Li) detectors; $H$, holmium sample; $S$, superconducting solenoid; $V$, vacuum Dewars; $O$, outline of cryostat. Distances are in cm.

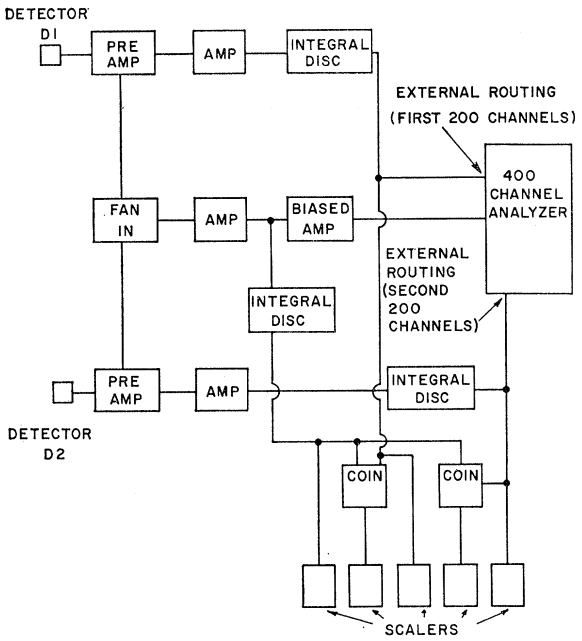


FIG. 8. Block diagram of electronics used in conjunction with detectors $D_1$ and $D_2$ in the measurements of the deformation and spin-spin effects.

parallel data recording systems which were checked against each other for consistency.

Despite the above precautions, long-term variations of as much as 10% in the ratio $R$ were observed when the Si(Li) detectors were operated at room temperature. These were removed by operating the detectors in individual vacuum dewars at liquid nitrogen temperature. During the actual experimental work, the long-term stability in the ratio $R$ was better than 0.2% over periods as long as 100 hours.

The holmium sample, detectors $D_1$ and $D_2$, and the copper collimator $C$ in Fig. 7 were carefully aligned along the beam axis with the aid of a transit. The dimensions of the detectors, the holmium sample, and the neutron collimator were chosen to minimize background without making the relative alignment of the various elements too critical. Figure 9 shows the placement of the two detectors $D_1$ and $D_2$ and the holmium sample $H$ relative to the collimated neutron beam. Measurements of the beam profile were made at various distances beyond the collimator, and a typical profile is shown in Fig. 10. The solid lines in Fig. 9 correspond to the full width at half maximum (FWHM) of the beam profiles. The ratio $R$ was expected to be independent of small changes in the positions of $D_1$, $D_2$, and $H$ when these elements were correctly aligned, and this was verified experimentally. A change of 2 mm in the position of $D_1$, $D_2$, or $H$ was required to produce a change greater than 2% in $R$, and the observed change in the position of any one of these elements during the course of the experiments was less than 0.25 mm. X-ray

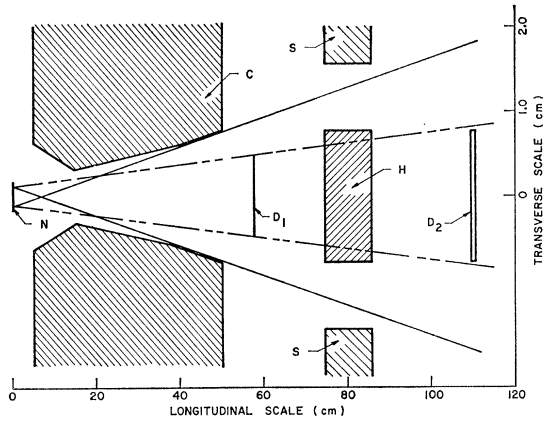


FIG. 9. Position of critical elements relative to the collimated neutron beam. The labeling of various elements is identical to that in Fig. 7. Note difference in horizontal and vertical scales.

photography was used to check the position of the holmium sample $H$.

The experimental arrangement for the measurement of the spin-spin effect is shown in Fig. 11. This measurement was performed only at $E_n=7.85$ MeV using the reaction $Be^9(\alpha,n)C^{12}$, since the reaction $T(d,n)He^4$ does not give significant neutron polarization at $E_d=250$ keV. The neutron source, detection system, holmium sample, and the SCONT system have been described. The angle between the neutron beam and the direction of the incident alpha beam was chosen as 45° to give maximum neutron polarization.[39] The dimensions of the pole pieces in Fig. 11 varied from a 15-cm-diam circular cross section at the coils to a 3.8-cm-wide×37-cm-long rectangular cross section at the gap. The total gap width was 1.6 cm. The integrated field of 332 kOe-cm along the neutron path produced a 90° precession of the neutron spins, as indicated in Fig. 11. The magnet power supply was provided with a switch, controlled from the data acquisition area, which automatically reversed the field direction. During the course of the experiment, the field in magnet $M$ was monitored by a Hall probe.

The copper collimator $C$ in Fig. 11 was made by electroforming copper over an aluminum mandril and chemically removing the aluminum. The collimator and other copper pieces were machined to fill in the space around the pole pieces of magnet $M$. The resulting neutron collimation was approximately equivalent to that obtained with the collimator of Fig. 7.

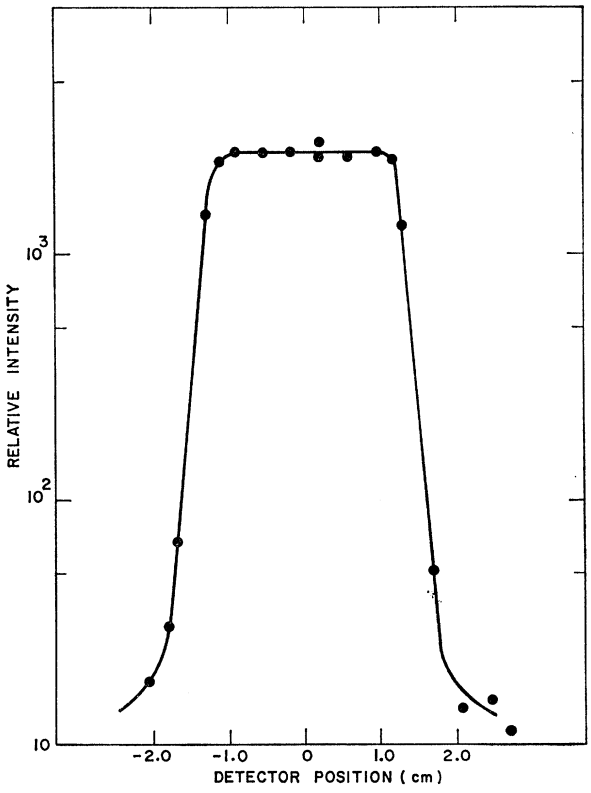


FIG. 10. Profile of collimated neutron beam taken at a distance 40 cm from the end of collimator $C$ in Figs. 7 and 9.

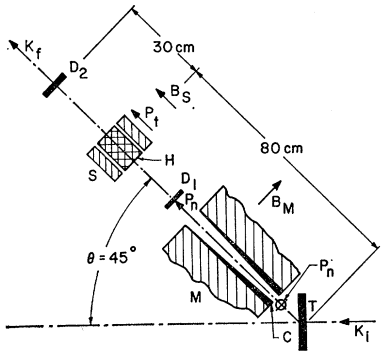


FIG. 11. Experimental arrangement for measurement of the spin-spin effect. $K_i$, incident $\alpha$ particle direction; $T$, $Be^9$ target; $C$, copper collimator; $M$, iron magnet; $D_1$, 80 mm²×2 mm Si(Li) detector; $D_2$, stack of two 200 mm²×2 mm Si(Li) detectors; $H$, holmium sample; $S$, superconducting solenoid; $K_f$, neutron direction; $P_n$, neutron polarization; $P_t$, $Ho^{165}$ polarization; $B_M$, field produced by magnet $M$; $B_S$, field produced by solenoid $S$. The figure is not drawn to scale.

## IV. EXPERIMENTAL PROCEDURE AND RESULTS

### A. Differential Elastic and Total Cross Section Measurements

The differential elastic-cross-section measurements were made in open geometry using the experimental set-up in Fig. 3. The bias for neutron detection was set just below the $Si^{28}(n,\alpha_0)Mg^{25}$ peak in the Si(Li) detector spectrum. For the $Be^9(\alpha,n)C^{12}$ reaction, the average neutron energy was 8.0 MeV and the energy spread was 450 keV. For the $H^3(d,n)He^4$ reaction, the average

[39] G. P. Lietz, S. F. Trevino, A. F. Behof, and S. E. Darden, Nucl. Phys. 67, 193 (1965).

TABLE III. Summary of measurements of $\Delta\sigma_{Def}$ at 8 and 15 MeV. $\Delta\alpha/\alpha$ is the percent change in the transmission of the sample. The results have been corrected for background and inscattering.

| $E_n$ (MeV) | $\Delta E_n$ (keV) | $\sigma_T$ (b) | $B_2/B_2(\max)$ | $\Delta\alpha/\alpha$ (%) | $\Delta\sigma_T/\sigma_T$ (%) | $\Delta\sigma_{Def}$ (mb) |
|---|---|---|---|---|---|---|
| 8.0 | 450 | 4.97±0.11 | 0.25±0.05 | +1.65±0.53 | −0.96±0.31 | −38±10 |
| | | | 0.25±0.05 | +0.69±0.53 | −0.40±0.31 | |
| | | | 0.25±0.05 | +1.82±0.65 | −1.05±0.38 | |
| 15.0 | 500 | 5.27±0.09 | 0.25±0.05 | +4.22±1.02 | −2.32±0.56 | −139±16[b] |
| | | | 0.25±0.05 | +5.40±0.93 | −2.97±0.51 | |
| | | | 0.17±0.04[a] | +3.22±0.62 | −1.77±0.34 | |

[a] This measurement was done at $M/M_\infty=0.47$ (see Sec. IV B).
[b] To obtain this result, the measurement at $M/M_\infty=0.47$ was multiplied by 1.5 and averaged with the other two measurements.

neutron energy was 15.0 MeV and the energy spread was 500 keV. The intrinsic detector resolution was about 150 keV, so the experimental resolution was determined mainly by the energy spread in the neutron beam.

A measurement of the cross section at a particular angle involved the following sequence of operations: (1) a measurement of the direct source intensity with the detector at 0°; (2) a measurement of the scattered intensity; (3) a measurement of background with the holmium sample removed. Several such cycles over periods of from one to five hours were taken at each angle. The long counter and current integrator were used to monitor the source intensity during each cycle. The three measurements described above make possible the extraction of an absolute cross section without absolute knowledge of either the detection efficiency or the neutron source intensity. Measurements were made on two different holmium samples: a 2.54-cm-diam×7.5-cm-long cylinder and a 2.54-cm-diam×2.5-cm-long cylinder. The shorter sample was used to give better angular resolution in the forward direction.

The experimental data were first reduced to give the quantity

$$\left[\frac{d\sigma}{d\Omega}(\theta)\right]_0=\frac{N_{\text{scatt}}}{N_{\text{inc}}n_s\Delta\Omega}, \tag{6}$$

where $N_{\text{scatt}}$ is the number of neutrons scattered into $\Delta\Omega$, the solid angle subtended by the detector, $N_{\text{inc}}$ is the number of incident neutrons per cm², and $n_s$ is the number of scattering nuclei. In making this reduction it was necessary to take into account the variation of detection efficiency with neutron energy, since the neutrons lose a small amount of energy in the scattering process. This point is discussed in much more detail in Ref. 40. The experimental results for $[d\sigma(\theta)/d\Omega]_0$ are plotted in Figs. 12 and 13. The uncertainties are primarily statistical, although there is a small contribution from uncertainties in the analysis. The relationship between $[d\sigma(\theta)/d\Omega]_0$ and the true differential elastic cross section involves corrections for finite geometry, multiple scattering, and inelastic scattering which is not completely resolved from the elastic scattering. These corrections are discussed in Appendix II. In the present case, 90% and 70%, respectively, of the inelastic scattering to the first and second excited states of $Ho^{165}$ was not resolved from the elastic scattering. The ratio of double to single scattering averaged about 15%.

The experimental arrangement for the total-cross-section measurements was quite straightforward. The measurements were made in open geometry using a Si(Li) detector. The results are given in Table III.

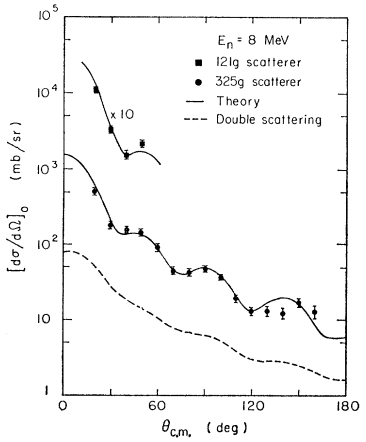


FIG. 12. Experimental angular distribution at $E_n=8$ MeV. The solid curves are theoretical fits to the quantity $[d\sigma(\theta)/d\Omega]_0$ defined in Eq. (6) of the text. The theoretical cross sections from which these curves were obtained are shown in Fig. 15. The dashed curve indicates the double scattering contribution.

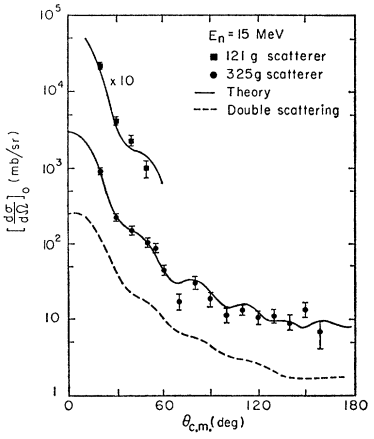


FIG. 13. Experimental angular distribution at $E_n=15$ MeV.

[40] E. G. Shelley, Ph.D. thesis, Stanford University, 1966 (unpublished).

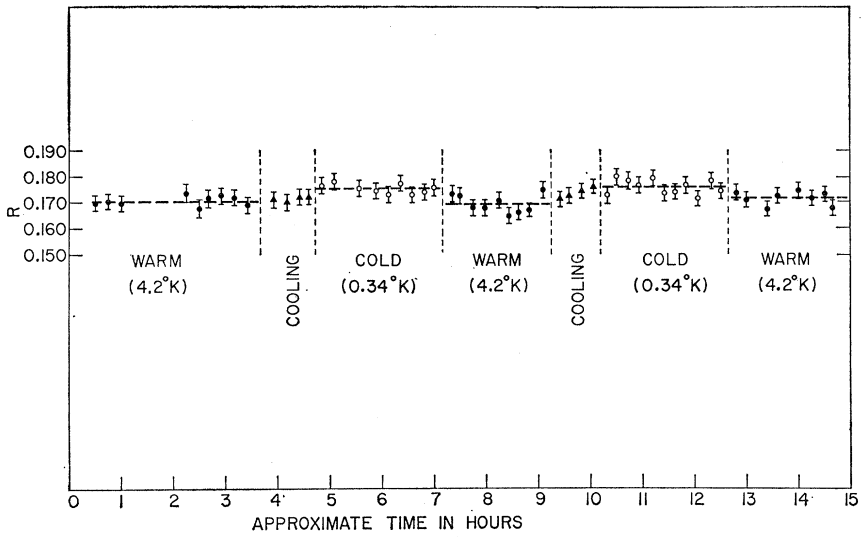


FIG. 14. Representative measurement of the deformation effect at $E_n=15$ MeV. $R$ is essentially proportional to the transmission of the holmium sample and is defined in Sec. III B. The absolute value of $R$ is not significant, but the percentage change in $R$ between the warm and cold periods is equal to the percentage change in the transmission of the sample, except for background and inscattering corrections which are discussed in Appendix III. The time sequence of operations is indicated by the abscissa in the figure.

Uncertainties are primarily statistical. The results have been corrected for background ($\approx 6\%$) and inscattering ($\approx 2\%$).

### B. Measurements of the Deformation Effect

A typical measurement of the deformation effect is shown in Fig. 14. The data were accumulated in 15 min intervals, and Fig. 14 indicates the time sequence of operations. As discussed in Sec. III B, the quantity actually measured as $R$, the ratio of counts recorded by the two Si(Li) detector systems $D_1$ and $D_2$ in Fig. 7. The bias for neutron detection is indicated in Fig. 4; the counting rate in detector $D_2$ was of the order of (3000 cts)/(15 min) interval above this bias during both the 8- and 15-MeV measurements. From each run such as that in Fig. 14 the quantity

$$\frac{\Delta R}{R}=2\left[\frac{R_{0.34°}-R_{4.2°}}{R_{0.34°}+R_{4.2°}}\right]$$

was determined by a two-parameter least-squares fit. The corresponding value of $\Delta\sigma_{\mathrm{Def}}$ was obtained from the relations in Appendix III which take into account corrections for background and inscattering. The background was determined in a separate measurement with the cryostat at room temperature by replacing the holmium sample with a total attenuator of copper; it amounted to $13\pm 3\%$ of the transmitted neutron flux for both the 8- and 15-MeV measurements. The inscattering correction was evaluated using theoretical cross sections calculated from the optical parameters listed in Figs. 15 and 16. This correction amounted to 1% and 3% at 8 and 15 MeV, respectively.

The results for $\Delta\sigma_{\mathrm{Def}}$ are summarized in Table III. The uncertainties are primarily statistical but include a small contribution from uncertainties in the background and inscattering corrections. Uncertainties in the nuclear orientation parameters are not included. The deformation effect depends upon only the even moments of the nuclear orientation and primarily on $B_2$, since in the present case $B_4$, $B_6$, and $B_8$ are small. At $E_n=15$ MeV, the theoretical calculation of Sec. V shows that $\Delta\sigma_{\mathrm{Def}}$ is a linear function of $B_2$ alone to a very good approximation, although this is not true in general. In Table III it will be noted that all measurements were done at the same nuclear orientation with the exception of one of the 15-MeV measurements. In this measurement, the field of the superconducting solenoid $S$ (Fig. 7) was reduced so that the average sample magnetization was $M/M_\infty=0.47$ rather than 0.70. The ratio between the result of this measurement and the average of the other two 15-MeV measurements is $0.67\pm 0.15$. The model described in Sec. II, which was used to evaluate $B_K$ for $K>1$, predicts that this ratio should be 0.67, the ratio of the two different magnetizations, and the verification of this prediction lends some additional support to the model. The mea-

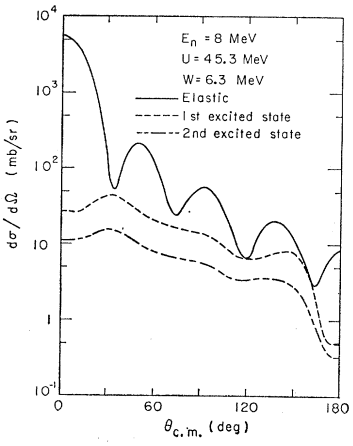


FIG. 15. Theoretical cross sections calculated for final choice of optical parameters at $E_n=8$ MeV.

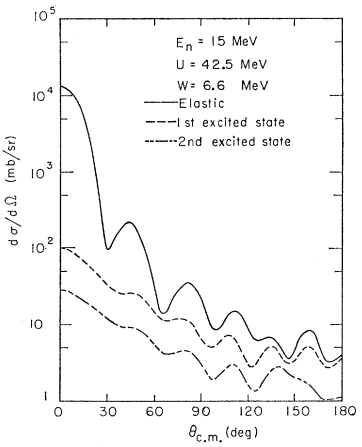


FIG. 16. Theoretical cross sections calculated for final choice of optical parameters at $E_n=15$ MeV.

surement at $M/M_\infty=0.47$ was multiplied by 1.5 and averaged with the two measurements at $M/M_\infty=0.70$ to obtain the final result for $\Delta\sigma_{\mathrm{Def}}$ at 15 MeV.

Two possible sources of error in the measurements of $\Delta\sigma_{\mathrm{Def}}$ will be considered briefly: (1) A volume change in the holmium sample due to the temperature change from 4.2°K to 0.34°K; (2) the presence of a spin-spin effect. The first has been shown to be small.[9] The change in the magnetization of our sample between 4.2 and 0.34°K was $<0.5\%$ which provides additional evidence that no significant volume change accompanies the change in temperature. The second source of error must be considered since the holmium sample was polarized. The neutron beam was initially unpolarized, however, so that any effects due to a spin-spin interaction would be of second order. Such effects may justifiably be neglected, since the first order spin-spin effect is quite small, both at $E_n=0.350$ MeV [8] and at $E_n=8$ MeV.

### C. Measurement of the Spin-Spin Effect

In the measurement of the spin-spin effect, the reaction $Be^9(\alpha,n)C^{12}$ was used as a polarized neutron source with $\theta=45°$, $E_n=7.85$ MeV, $\Delta E_n=330$ keV. The polarization of neutrons produced in this reaction has been measured by Lietz *et al.*[39] At $\theta=45°$, $E_n=7.90$, and $\Delta E_n=300$ keV, they report an average neutron polarization $0.36\pm0.02$ where the sign of the polarization is given by the Basel convention. Using this result as a basis and applying a correction for the small differences in $E_n$ and $\Delta E_n$, we obtained $0.34\pm0.02$ for the average polarization in our neutron beam. After the neutrons have passed through magnet $M$ in Fig. 11 the polarization axis is parallel to $\mathbf{K}_f$ and the relative orientation of the neutron and $Ho^{165}$ spins depends on the relative direction of the fields in magnet $M$ and solenoid $S$. Data were recorded in 15-min intervals and the field in magnet $M$ was reversed at the end of each interval by means of the automatic reversing switch described in Sec. III B. The field in solenoid $S$ was reversed at 8-h intervals. As in the measurements of the deformation effects, the quantity actually recorded was $R$, the ratio of counts in the two Si(Li) detector systems. The quantity $\sigma_{\uparrow\uparrow}-\sigma_{\uparrow\downarrow}$, where $\sigma_{\uparrow\uparrow}$ and $\sigma_{\uparrow\downarrow}$ refer to the total cross sections for the parallel and antiparallel spin configurations, was derived using the expressions in Appendix III. Corrections for background and inscattering amounted to 18% and $<2\%$, respectively.

TABLE IV. Summary of measurement of $\Delta\sigma_{ss}$ at 7.85 MeV.

| $E_n$ (MeV) | $\Delta E_n$ (keV) | $P_n$ | $B_1/B_1(\max)$ | $\Delta\sigma_{ss}$ (mb) |
|---|---|---|---|---|
| 7.85 | 330 | 0.34±0.02 | 0.55±0.03 | +5±9 |
| | | | 0.06 | +2±9 } +3±13 |

The procedure of reversing both the neutron and $Ho^{165}$ spin directions should result in the cancellation of most instrumental asymmetries. This point was checked by a measurement with the holmium sample at 4.2°K. The results of the measurements are presented in Fig. 17, where each point represents a consensus of the individual 15 min runs taken over one 8-h period. From the measurements at 0.34°K $[B_1/B_1(\max)=0.55]$ we obtain $\sigma_{\uparrow\uparrow}-\sigma_{\downarrow\uparrow}=5\pm9$ mb; from the measurements at 4.2°K $[B_1/B_1(\max)=0.06]$ we obtain $\sigma_{\uparrow\uparrow}-\sigma_{\downarrow\uparrow}=2\pm9$ mb. Taking the 4.2°K measurement as a measure of the instrumental asymmetry and combining the two results gives $\sigma_{\uparrow\uparrow}-\sigma_{\uparrow\downarrow}=3\pm13$ mb. This result is to be interpreted with reference to a neutron ensemble having a polarization of 0.34 and an ensemble of $Ho^{165}$ nuclei described by the orientation parameters in Table I. The uncertainties quoted for $\sigma_{\uparrow\uparrow}-\sigma_{\uparrow\downarrow}$ are statistical, since all other sources of uncertainty are negligible. A summary of all information pertinent to the spin-spin measurement is given in Table IV.

Since the holmium sample was not magnetically saturated, the neutron beam experienced a net depolarization in passing through the sample. This depolarization

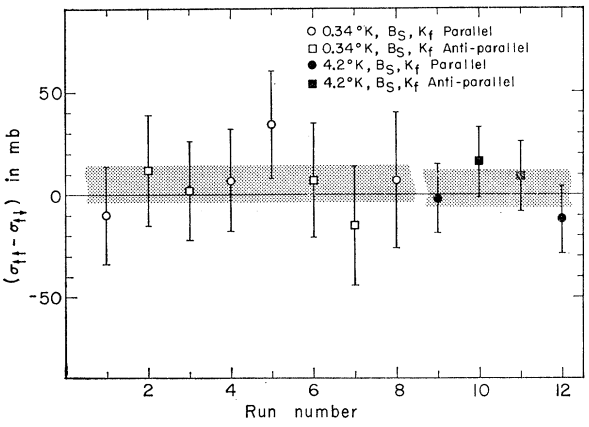


FIG. 17. Results of measurement of spin-spin effect. Each point represents the consensus of 8 h of actual running time, during which the relative spin orientation was reversed at 15-min intervals. The average of the 0.34°K measurements is 5±9 mb; the average of the 4.2°K measurements is 2±9 mb.

can be estimated using the model described in Sec. II if the average size of the single crystallites in the polycrystalline metal is known. An upper limit of 250$\mu$ for this size was estimated from the grain size revealed by micrographs of polished and etched surfaces. This led to a value less than 1% for the depolarization, and this correction was neglected.

## V. THEORETICAL ANALYSIS

### A. Method

The neutron differential and total cross sections were obtained from a coupled-channels calculation[41–43] using the adiabatic approximation.[44,45] A detailed formulation of the problem has been given previously.[7] In the adiabatic approximation the members of the ground-state rotational band are assumed to be degenerate and the coupling between all of them is automatically taken into account. The condition for the validity of the approximation is[45]:

$$kR_0\Delta E/E \ll 1, \tag{7}$$

where $k$ is the wave number of the incident neutron, $E$ its energy, $R_0$ the radius of the nucleus, and $\Delta E$ the excitation energy of the excited state of the target. This criterion is well satisfied in the case of $Ho^{165}$ for neutron energies above 1 MeV, since $kR_0\Delta E/E<0.14$ for the 0.095-MeV rotational state.

The potential used in the calculation was

$$V(R,\theta')=-Uf(r,R(\theta'),a)+iW\left[4\bar{a}\frac{\partial f}{\partial r}(r,\bar{R}(\theta')),\bar{a}\right] \tag{8}$$

where

$$f(r,R(\theta'),a)=\{\exp[(r-R(\theta'))/a]+1\}^{-1},$$
$$R(\theta')=r_0A^{1/3}[1+\beta Y_{20}(\theta')]. \tag{9}$$

Here $\theta'$ is defined with respect to the nuclear symmetry axis. The potential was expanded in Legendre polynomials up through $L=4$, by carrying out angular integrations numerically at each point $r$.

To simplify the calculation, a spin-orbit term was not included in the optical potential. Such a term is necessary to explain the results of polarization measurements, but does not significantly affect scattering calculations. In the analysis described here, good fits to all the data were obtained. The inclusion of a spin-orbit term would be expected to alter slightly the values of $U$ and $W$, giving the best fit to the angular distribution data and $\Delta\sigma_{\mathrm{Def}}$. Davies and Satchler[15] have previously pointed out that the effects of spin-orbit coupling on the spin-spin interaction (the interaction which gives rise to $\Delta\sigma_{\mathrm{ss}}$) are small.

The optical model parameters were obtained by fitting the differential elastic scattering from an unpolarized target. An optical-model parameter search program written by Perey was used together with the coupled channel code. Both programs were modified to include the effects of finite geometry, multiple scattering, and direct inelastic scattering, as discussed in Appendix II. That is, for a particular set of optical parameters, the quantity $[d\sigma(\theta)/d\Omega]_0$ defined in Eq. (6) was calculated as well as the theoretical cross sections. It was assumed that compound elastic scattering was negligible at the energies involved. The search was performed in parameters $U$ and $W$ only. The other optical parameters were held constant at the consensus values[46,47] for spherical nuclei:

$$r_0=1.25\ \mathrm{F},\quad a=0.65\ \mathrm{F},$$
$$\bar{r}_0=1.25\ \mathrm{F},\quad \bar{a}=0.47\ \mathrm{F}. \tag{10}$$

The quadrupole deformation parameter was fixed at the accepted value[1–4] of $\beta=+0.3$.

In the search procedure, a calculation was first performed with the coupled-channel code using a trial set of optical parameters; the resulting differential cross sections were used to generate "pseudodata" from the experimental data. That is, we may write

$$\sigma_{\mathrm{pseudo}}(\theta)=\sigma_{\mathrm{exp}}(\theta)-\sigma_{\mathrm{th}}{}^{(1)}(\theta)+\sigma_{\mathrm{th}}{}^{(2)}(\theta), \tag{11}$$

where $\sigma_{\mathrm{exp}}(\theta)$ is the experimental value of the quantity $[d\sigma(\theta)/d\Omega]_0$ as defined in Eq. (6) and Eq. (A3) in Appendix II, $\sigma_{\mathrm{th}}{}^{(1)}(\theta)$ is the theoretical value of this quantity for $\beta=0.3$, and $\sigma_{\mathrm{th}}{}^{(2)}(\theta)$ is the theoretical value of this quantity for $\beta=0$. The values for $\sigma_{\mathrm{pseudo}}(\theta)$ were inserted into the optical-model search program to generate a new set of optical parameters and the process was repeated until convergence was reached. This procedure proved much more economical than incorporating as earch routine directly into the coupled-channel code, and only three iterations were actually required to obtain convergence.

The total cross sections $\sigma_M(\mathrm{tot})$ for the cases of the target nucleus in different initial states $I_z=M$ were calculated from the forward scattering amplitudes using the optical theorem. We shall write expressions for $\Delta\sigma_{\mathrm{Def}}$ and $\Delta\sigma_{\mathrm{ss}}$ only for an axially symmetric distribution of nuclear spins. As discussed in Sec. II, only the initial population densities $P_M$ are required to specify the nuclear orientation. The deformation effect, or difference between the total cross sections for a polarized and an unpolarized target, is given by

$$\Delta\sigma_{\mathrm{Def}}=\sum_M[P_M-1/(2I+1)]\sigma_M(\mathrm{tot}) \tag{12}$$

[41] B. Buck, A. P. Stamp, and P. E. Hodgson, Phil. Mag. **82**, 1805 (1963).
[42] B. Margolis and E. S. Troubetzkoy, Phys. Rev. **106**, 105 (1957).
[43] D. M. Chase, L. Wilets, and A. R. Edmonds, Phys. Rev. **110**, 1080 (1958).
[44] D. M. Chase, Phys. Rev. **104**, 838 (1956).
[45] S. J. Drozdov, Zh. Eksperim. i Teor. Fiz. **36**, 1875 (1959) [English transl.: Soviet Phys.—JETP **9**, 1335 (1959)].
[46] F. Bjorklund and S. Fernbach, Phys. Rev. **109**, 1295 (1958).
[47] F. G. Perey and B. Buck, Nucl. Phys. **32**, 353 (1962).

The change in the forward elastic scattering cross section resulting from polarization is obtained by substituting $\sigma_M(\theta=0)$ in place of $\sigma_M(\text{tot})$ in Eq. (12). This quantity is needed in the evaluation of the inscattering correction discussed in Appendix III.

For the calculation of the spin-spin effect, the following term was added to the potential:

$$-V_{ss}f(r,r_0A^{1/3},a)\boldsymbol{\sigma}\cdot\mathbf{I}/I \qquad (13)$$

where $f$ is defined in Eq. (9). The possibility of neutron spin flip by the $\mathbf{I}\cdot\boldsymbol{\sigma}$ interaction was neglected, and cannot be included if the adiabatic approximation is used. Since a strong coupling calculation for a spin $\frac{7}{2}$ nucleus without the adiabatic approximation is impractical at energies of several MeV, the only real alternative to the present approach is a DWBA calculation similar to that of Davies and Satchler.[15] This approach treats the neutron spin flip correctly, but involves other approximations which do not exist in the present calculation. It is reassuring to note that at 14 MeV the two methods of calculation are in good agreement [$\Delta\sigma_{ss}$(DWBA) $=-7$ mb to be compared with the value $-7$ mb at $E_n=14$ MeV in Fig. 21].

The spin-spin effect is defined to be the difference between the total cross sections for the parallel and antiparallel configurations of the target and incident neutron polarizations. If we define $\sigma_{\uparrow\uparrow M}(\text{tot})$ as the calculated total cross section for nuclei in the state $I_z=M$ when the term $-V_{ss}f(r,r_0A^{1/3},a)$ is added to the real potential and $\sigma_{\uparrow\downarrow M}(\text{tot})$ as the corresponding total cross section when $+V_{ss}f(r,r_0A^{1/3},a)$ is added to the real potential, then $\Delta\sigma_{ss}$ may be written as

$$\Delta\sigma_{ss}=P_n\sum_{M>0}(P_M-P_{-M})\times[\sigma_{\uparrow\uparrow M}(\text{tot})-\sigma_{\uparrow\downarrow M}(\text{tot})]M/I \qquad (14)$$

where $P_n$ is the neutron beam polarization. In the above expression, it is assumed that $\Delta\sigma_{ss}$ is a linear function of $V_{ss}$; this assumption is well justified for the range of $V_{ss}$ which was considered since $V_{ss}/U\ll 1$.

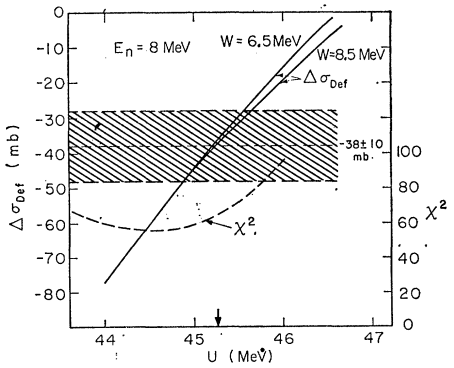


FIG. 18. Plot of calculated value of $\Delta\sigma_{\text{Def}}$ versus $U$ (scale on left) and $\chi^2$ for angular-distribution fit versus $U$ (scale on right) at $E_n=8$ MeV. To obtain the $\chi^2$ versus $U$ curve, $W$ was allowed to vary to minimize $\chi^2$ for a fixed value of $U$.

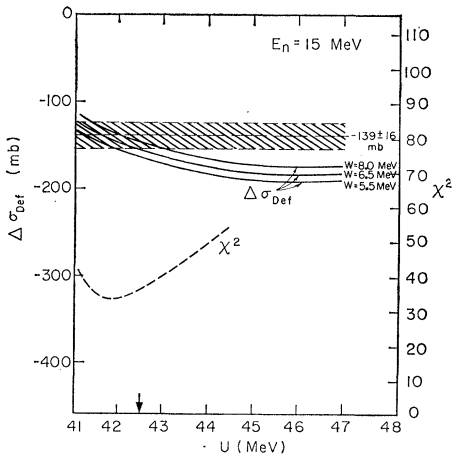


FIG. 19. Plot of $\Delta\sigma_{\text{Def}}$ versus $U$ and $\chi^2$ versus $U$ at $E_n=15$ MeV.

### B. Results of Calculations

Figures 18 and 19 show plots of $\chi^2$ versus $U$ for the angular distributions. The parameter $W$ was allowed to vary in order to minimize $\chi^2$. The same figures show calculated values of the deformation effect plotted against $U$, together with shaded areas which represent a range of one standard deviation on either side of the experimental value. These figures were used to arrive at final values for $U$ and $W$ at 8 and 15 MeV. It can be seen that the minimum in $\chi^2$ is quite shallow so that the angular distributions by themselves do not establish precise values for $U$ and $W$.

At $E_n=8$ MeV, the minimum in $\chi^2$ occurs at $U=44.6$ MeV. However, as can be seen, the calculated value of $\Delta\sigma_{\text{Def}}$ depends strongly on $U$ (although very little on $W$) and the value $U=45.3$ MeV is required to give agreement with the experimental measurement of $\Delta\sigma_{\text{Def}}$. The total cross section $\sigma_t$ does not depend strongly on either $U$ or $W$ and is of little value in establishing the values of these parameters. Therefore, the value 45.3 MeV was chosen for $U$. The corresponding value of $W$ which minimizes the $\chi^2$ for the angular distribution is 6.3 MeV. The resulting $\chi^2$ is not significantly worse than the best possible $\chi^2$. Therefore, at $E_n=8$ MeV, the final result is

$$U=45.3\text{ MeV},\quad W=6.3\text{ MeV},$$
$$\sigma_t(\text{theory})=4.92\text{ b},$$
$$\Delta\sigma_{\text{Def}}(\text{theory})=-37.3\text{ mb}.$$

At $E_n=15$ MeV, the dependence of $\Delta\sigma_{\text{Def}}$ on $U$, is not strong. From Fig. 19 it can be seen that the value $U=41.7$ MeV corresponds to the minimum in $\chi^2$ and also gives good agreement with the experimental measurement of $\Delta\sigma_{\text{Def}}$. However, the calculated value of $\sigma_t$ is more than one standard deviation from the experimental value. If the parameters $U=42.5$ MeV, $W=6.6$ MeV are chosen, the $\chi^2$ for the angular distribution is not significantly increased and the calculated values

for both $\Delta\sigma_{\mathrm{Def}}$ and $\sigma_t$ lie within one standard deviation of the experimental values. Therefore, at $E_n=15$ MeV, the final result is

$$U=42.5 \text{ MeV}, \quad W=6.6 \text{ MeV},$$
$$\sigma_t(\text{theory})=5.37 \text{ b},$$
$$\Delta\sigma_{\mathrm{Def}}(\text{theory})=-155 \text{ mb}.$$

The fits to the angular distribution data which resulted from the final choice of optical parameters are shown in Figs. 12 and 13. The cross sections are plotted in Figs. 15 and 16. The theoretical values for $\sigma_t$ and $\Delta\sigma_{\mathrm{Def}}$ may be compared with the experimental values in Table III.

A calculation of the deformation effect and the spin-spin effect over a range of energies including those at which the present experimental measurements were made, is shown in Figs. 20 and 21, respectively. The calculations were done for three cases: $U=45.2$, $W=3$; $U=42.5$, $W=6.5$; and a smooth energy variation in $U$ and $W$. The smooth variation included the values $U=45.2$, $W=3$ at 0.350 MeV,[8] $U=45.3$, $W=6.3$ at 8 MeV, and $U=42.5$, $W=6.6$ at 15 MeV. At the lower end of the energy range, the validity of the adiabatic approximation is in some doubt, since the left hand side of Eq. (7) becomes 0.23 for $E_n=350$ keV. The

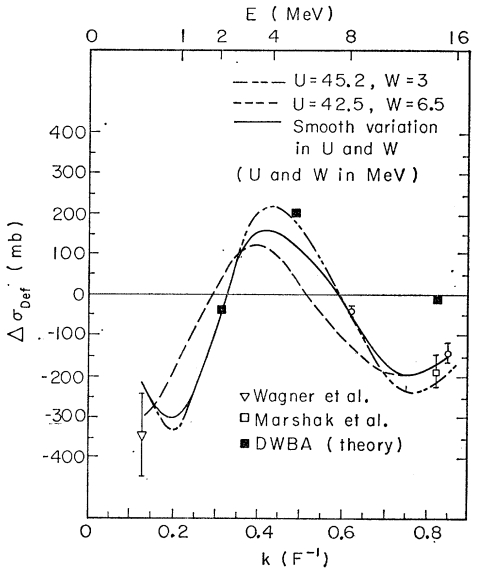


FIG. 20. Calculation of $\Delta\sigma_{\mathrm{Def}}$ as a function of neutron energy. The nuclear orientation is that of the present experiment. The solid curve corresponds to the most probable choice of optical parameters: i.e., a smooth interpolation between the best values of $U$ and $W$ at 0.350, 8, and 15 MeV. The other curves correspond to arbitrary choices for $U$ and $W$ and are included to give some idea of the dependence of $\Delta\sigma_{\mathrm{Def}}$ on these parameters. The adjustment in the points taken from Refs. 8 and 9 was made as follows: $\Delta\sigma_{\mathrm{Def}}$ was calculated for the nuclear orientation of Refs. 8 and 9 as well as for the present orientation, and the experimental points were corrected by the ratio of the two calculated values. This ratio was approximately $-1$. The 8- and 15-MeV points are from the present experiment.

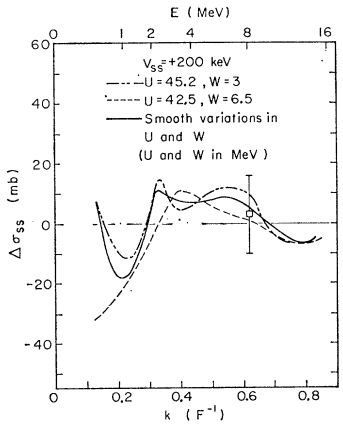


FIG. 21. Calculation of $\Delta\sigma_{ss}$ as a function of neutron energy. The calculated curves correspond to the nuclear orientation of the present experiment, a neutron polarization of 0.34 with polarization axis parallel to the neutron beam direction, and the value $V_{ss}=+200$ keV. The curves can be directly scaled for different values of $V_{ss}$ and different neutron polarizations. The experimental point is from the present experiment.

results for $\Delta\sigma_{\mathrm{Def}}$ and $\Delta\sigma_{ss}$ differ markedly from the theoretical calculations of Tamura[8,11] at $E_n=350$ keV.

In the calculation of Tamura, the coupling between the 0.095-MeV first excited state and the ground state of $Ho^{165}$ was treated exactly and a spin-orbit term was included in the optical potential. However, the coupling to higher excited states was not included and the partial-wave expansion was cut off at $l=3$. In the present calculation, it was found necessary to include partial waves up to $l=8$ to obtain convergent results for $\Delta\sigma_{\mathrm{Def}}$ and $\Delta\sigma_{ss}$ at $E_n=350$ keV. For example, when $l_{\max}$ was increased from 4–8 in our calculation, $\Delta\sigma_{\mathrm{Def}}$ decreased by 50% and $\Delta\sigma_{ss}$ changed sign, although no significant change was observed when $l_{\max}$ was increased from 8–10. As has been pointed out, the adiabatic approximation automatically includes effects of coupling to all members of the ground state rotational band and between all partial waves. Its validity at $E_n=350$ keV is in some doubt, because it does not differentiate between real and virtual states, although this probably causes less error than ignoring the coupling to the virtual states altogether. It is felt that an exact coupling calculation similar to that of Tamura in which more channels and more partial waves are included is needed for $E_n=350$ keV.

## VI. CONCLUSIONS

### A. Deformation Effect

The existing data on $\Delta\sigma_{\mathrm{Def}}$, together with the calculated curves, are displayed in Fig. 20. The theoretical curves are calculated for nuclear orientation defined by the orientation parameters in Table I. The experimental points of Wagner *et al.*[8] and Marshak *et al.*,[9] which were measured with a different nuclear orientation, have been suitably adjusted (see explanation in figure caption).

The coupled-channel formalism in adiabatic approximation gives a good account of all existing data on $\Delta\sigma_{\mathrm{Def}}$. The angular distribution data at $E_n=8$ and 15 MeV from the present experiment are also fitted quite adequately. The $\chi^2$ values for the fits in Figs. 12 and 13

are 62 for 18 degrees of freedom at 8 MeV and 36 for 18 degrees of freedom at 15 MeV. A large contribution to the $\chi^2$ comes from a few backward angles, often a troublesome region for optical-model fits. The calculated values of the total cross section, $\sigma_t=4.92$ b at $E_n=8$ MeV, and $\sigma_t=5.37$ b at $E_n=15$ MeV, are in good agreement with the experimental values listed in Table III. No attempt has been made to fit the angular distribution data of Wagner *et al.*[8] at $E_n=350$ keV with the present calculation, and it may be that an exact coupling calculation is required to fit all the data available at this energy. The exact coupling calculation of Tamura does give good agreement with all the experimental data at $E_n=350$ keV, although it is felt that the results of this calculation might be significantly changed by the inclusion of higher partial waves and more channels as discussed in Sec. V.

The DWBA calculation of Davies and Satchler, while in reasonable agreement with the present calculation of $\Delta\sigma_{\mathrm{Def}}$ at neutron energies of 2 and 5 MeV, differs strongly from both the present calculation and the experimental results at $E_n=14$ MeV. The failure of the DWBA at 14 MeV is somewhat puzzling unless the agreement at 2 and 5 MeV is accidental. In any case, it appears probable that the DWBA approach is inadequate when the nuclear deformation is as large as 0.3. The black-nucleus approximation has been shown to be in disagreement with the experimental results for $\Delta\sigma_{\mathrm{Def}}$ at $E_n=14$ MeV.[9] Therefore, a coupled-channel calculation appears to be the only approach capable of explaining the existing data on the deformation effect in $Ho^{165}$.

The simple periodic structure of the curves in Fig. 20 is quite interesting, since this qualitative feature remains essentially unaltered by rather gross changes in the optical parameters $U$ and $W$. That $\Delta\sigma_{\mathrm{Def}}$ does, in fact, change sign in the region $E_n=4$ MeV is strongly suggested by the experimental point at 8 MeV but a direct experimental verification of this fact would be extremely valuable. Some additional insight into the structure of the curves in Fig. 20 may be gained from Fig. 22, where calculated values of $\sigma_M(\mathrm{tot})$ are plotted as a function of energy for each of the possible $M$ states. It will be noted that the curves show broad "resonances" which are familiar features in total-cross-section curves and have recently been explained in terms of a nuclear "Ramsauer effect" by Peterson[48] and by McVoy.[49] However, the position and amplitude of a particular "resonance" varies in going from the $M=\frac{7}{2}$ state to the $M=\frac{1}{2}$ state and these variations produce the structure of the curves in Fig. 20. The oscillatory behavior of $\Delta\sigma_{\mathrm{Def}}$ as a function of energy can thus be understood as a more subtle manifestation of a well known phenomenon. From this point of view one would predict more oscillations for $\Delta\sigma_{\mathrm{Def}}$ in the region $E_n>15$ MeV although this prediction is purely conjecture at this time.

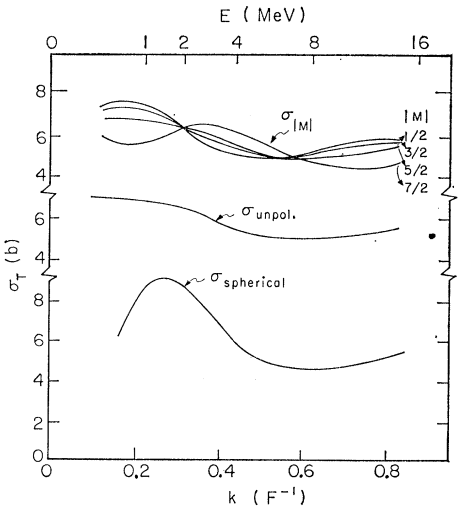


FIG. 22. Plot of $\sigma_M(\mathrm{tot})$ as a function of neutron energy. The optical parameters are those used to calculate the solid curve in Fig. 20.

At $E_n=8$ MeV, as has been mentioned, the calculated value of $\Delta\sigma_{\mathrm{Def}}$ is strongly dependent on $U$, the strength of the real part of the optical potential. This is not surprising since Fig. 20 shows that 8 MeV is close to the energy at which $\Delta\sigma_{\mathrm{Def}}$ changes sign. This feature has been used to establish narrow limits on $U$ and $W$ which are important in the interpretation of the measurement of $\Delta\sigma_{\mathrm{ss}}$ at 8 MeV. Conversely, at $E_n=14$ and 15 MeV, we are close to a maximum in the amplitude of $\Delta\sigma_{\mathrm{Def}}$ and the dependence on $U$ and $W$ is weak. Therefore, an estimate of the quadrupole deformation parameter $\beta$ can be extracted from the 14- and 15-MeV measurements. The result is $\beta=0.3\pm0.05$,[50] which is in good agreement with all previous determinations of $\beta$ although the uncertainty is considerably greater than that obtained in recent Coulomb excitation measurements.[2,4] Nevertheless, it is significant that this determination of $\beta$, which is sensitive to both the neutron and proton distributions, agrees so well with the Coulomb excitation measurements in which only the charge deformation was directly measured.

### B. Spin-Spin Effect

In Fig. 21 curves of $\Delta\sigma_{\mathrm{ss}}$ as a function of neutron energy are plotted for $V_{\mathrm{ss}}=+200$ keV, a neutron polarization of 0.34, and a nuclear orientation described by the parameters in Table I. The curves of $\Delta\sigma_{\mathrm{ss}}$ for

[48] J. M. Peterson, Phys. Rev. **125**, 955 (1962).
[49] K. W. McVoy, Phys. Letters **17**, 42 (1965).

[50] To obtain the uncertainty limits quoted here, $\Delta\sigma_{\mathrm{Def}}$ was assumed to be directly proportional to $\beta$. The uncertainty in $B_2/B_2(\mathrm{max})$ was combined with the statistical uncertainty in the present measurement at 15 MeV. The resulting uncertainty was 22% and, together with the 14-MeV measurement for which the uncertainty is also 22%, led to a 16% uncertainty in the value of $\beta$.

different choices of optical parameters show considerable variation, and illustrate the importance of obtaining precise limits on $U$ and $W$ before attempting an interpretation of the $\Delta\sigma_{ss}$ measurement. From the measurements of the angular distribution and total cross section plus the measurement of $\Delta\sigma_{Def}$, the acceptable limits on $U$ and $W$ at $E_n=8$ MeV may be set at $U=45.2\pm0.3$ MeV, $W=6.3\pm0.5$ MeV. The measurement of $\Delta\sigma_{Def}$ primarily establishes limits for $U$. The remaining data then restrict the acceptable range of $W$. These limits are quite small compared to the changes in $U$ and $W$ which correspond to the different curves in Fig. 21.

If the form of the spin-spin potential is chosen as that defined by Eq. (13) of Sec. V, the acceptable limits on the strength of the potential are $-340$ keV$<V_{ss}<540$ keV. This result is consistent with the result of Wagner *et al.*,[8] $-460$ keV$<V_{ss}<980$ keV, obtained from a measurement of $\Delta\sigma_{ss}$ at $E_n=350$ keV. Both results indicate that the spin-spin interaction is at least an order of magnitude weaker than the spin-orbit interaction, and it is not surprising that no evidence for its existence has been found in data taken with an unpolarized target.[18] A microscopic model of the spin-spin interaction, in which the strength $V_{ss}$ is estimated from the known spin-dependence in the two-body interaction (see Appendix IV), predicts that $V_{ss}$ should be of the order of $+60$ keV which is well within the limits imposed by the present experiment and the experiment of Wagner *et al.*[8]

In a recent experiment, Kobayashi *et al.*[51] have measured the value $\Delta\sigma_{ss}=-128\pm66$ mb at $E_n=920$ keV. The neutron polarization in this experiment was 0.30, and the first moment of the nuclear orientation was 0.31. The large value of $\Delta\sigma_{ss}$, according to the analysis of Kobayashi *et al.*, leads to the result $V_{ss}=10\pm5.2$ MeV. Even allowing for uncertainties in analysis, it is apparent that the value $-128$ mb for $\Delta\sigma_{ss}$ at $E_n=920$ keV requires a value of $V_{ss}$ much larger than that which could be explained on the basis of any microscopic model, and much larger than that suggested by previous experimental evidence. It should be pointed out, however, that the instrumental asymmetry measurement of Kobayashi *et al.*, in which no target polarization was present, gave the result $-38\pm60$ mb. If this result is statistically combined with their polarized target measurement, the net result is $\Delta\sigma_{ss}=-90\pm90$ mb, consistent with a small value for $\Delta\sigma_{ss}$ and for $V_{ss}$. The data of Kobayashi *et al.* certainly indicate that the region $E_n=920$ keV should be further investigated, although it is felt, for the reason given above, that their data are not inconsistent with the limits on $V_{ss}$ imposed by the present experiment.

[51] S. Kobayashi, H. Kamitsubo, K. Katori, A. Uchida, M. Imaizumi, and K. Nagamine, Progr. Theoret. Phys. (Kyoto) (to be published).

## ACKNOWLEDGMENTS

The authors wish to thank P. R. Bevington for making available the Monte-Carlo Program MANIAC and for aiding in the adaptation of this program to the needs of the present calculations. We also thank W. E. Meyerhof, W. A. Little, and S. S. Hanna for continued help and encouragement during the course of this work. The assistance of the technical staff of the Stanford University Nuclear Structure Group is also gratefully acknowledged.

## APPENDIX I: MAGNETIZATION MEASUREMENTS

If a cylinder of homogeneous material is magnetized in a uniform external magnetic field $H_0$ which is parallel to the axis of the cylinder, the relationship between $H_0$, $M$, $B$, and $H$ at the center of the cylinder is given by the following equations:

$$\mu_0 H=\frac{\mu_0 H_0-NB}{1-N},\qquad M=\frac{B-\mu_0 H_0}{1-N}. \tag{A1}$$

$N$ is called the demagnetizing factor, and its value, $N=N_c$, has been tabulated as a function of the permeability and the dimensions of the cylinder.[52]

If a gap of width $d$ is introduced at the center of the cylinder, the additional demagnetizing field of the gap must be taken into account. In this case, $N=N_c+f(M,d/D,L)$ where $f(M,d/D,L)$ is some function of the magnetization $M$ and the dimensions. $L$ denotes the length of the cylinder and $D$ its diameter. If $(d/D)\ll1$, $f(M,d/D,L)\approx d/D$ to a very good approximation.[32] We then have $N=N_c+(d/D)$; the value of $N$ for the geometry illustrated in Fig. 1 was 0.06. Although the external magnetic field in Fig. 1 was not constant over the entire length of the cylinder, the non-uniformity was less than 5% within a radius of 2.5 cm from the center. The error introduced in the estimate of $N$ by the non-uniformity in $H_0$ along the length of the cylinder was not serious, since $N$ was almost negligible in any case.

## APPENDIX II: CORRECTIONS TO EXPERIMENTAL ANGULAR DISTRIBUTIONS

The quantity $[d\sigma(\theta)/d\Omega]_0$ defined by Eq. (6) is related to the true differential elastic cross section as follows. We write

$$\left[\frac{d\sigma}{d\Omega}(\theta)\right]=\left[\frac{d\sigma}{d\Omega}(\theta)\right]_{el}+\sum_j \gamma_j\left[\frac{d\sigma}{d\Omega}(\theta)\right]_{in,j} \tag{A2}$$

[52] R. M. Bozorth, *Ferromagnetism* (D. Van Nostrand, Inc., New York, 1951).

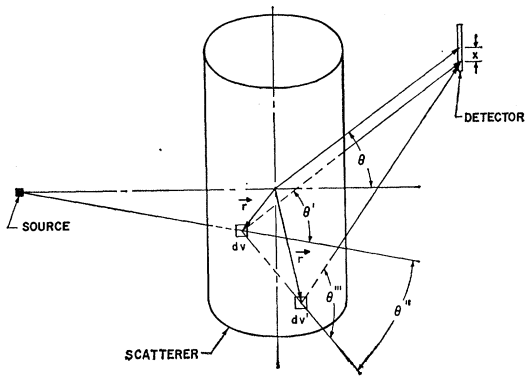


FIG. 23. Scattering geometry. The figure is not drawn to scale. The various quantities which enter into Eq. (A3) are indicated.

where $[d\sigma(\theta)/d\Omega]_{el}$ is the differential elastic cross section, $[d\sigma(\theta)/d\Omega]_{in,j}$ is the differential inelastic cross section for excitation of the $j$th excited state, and $\gamma_j$ is the fraction of inelastic scattering to this state which is not resolved from elastic scattering. In the present case, the inelastic term was composed of 90% and 70%, respectively, of the cross sections for direct inelastic scattering to the first two excited states in $Ho^{165}$. Then, with reference to Fig. 23,

$$\left[\frac{d\sigma}{d\Omega}(\theta)\right]_0 = \int dx \int dV \left[F(\varphi)G_{SS}(\mathbf{r},x,\theta)\frac{d\sigma}{d\Omega}(\theta')\right] + \int dx \int dV \int dV' \left[F(\varphi)G_{DS}(\mathbf{r},\mathbf{r}',x,\theta) \times \frac{d\sigma}{d\Omega}(\theta'')\frac{d\sigma}{d\Omega}(\theta''')\right] + \cdots \quad \text{(A3)}$$

The first integral in Eq. (A3) describes the smearing effect arising from the finite size of the scatterer, and the second integral is the correction for double scattering. Higher order scattering was assumed to be isotropic, and its intensity was estimated from the average ratio of double to single scattering. The function $F(\varphi)$ describes the variation in source intensity as a function of the angle $\varphi$. The quantities $G_{SS}(\mathbf{r},x,\theta)$ and $G_{DS}(\mathbf{r},\mathbf{r}',x,\theta)$ are geometrical factors. The derivation of exact analytical expressions for these quantities is tedious but quite straightforward.[40]

Although Eq. (A3) may be inverted by an iterative procedure to obtain $[d\sigma(\theta)/d\Omega]$ from the experimental values for $[d\sigma(\theta)/d\Omega]_0$, this was not necessary for our purpose. Instead, the theoretical cross sections were inserted into the integrals in Eq. (A3) and the resulting theoretical curves for $[d\sigma(\theta)/d\Omega]_0$ were compared with the experimental results. The search procedure for obtaining the optical parameters giving the best fit to the experimental data is described in Sec. V. The integrals in Eq. (A3) were evaluated with the aid of a computer program[53] utilizing Monte-Carlo techniques.

[53] P. R. Bevington and G. A. Pettit, Nucl. Instr. Methods 44, 341 (1966).

## APPENDIX III: BACKGROUND AND INSCATTERING CORRECTIONS TO MEASUREMENTS OF THE DEFORMATION AND SPIN-SPIN EFFECTS

In general, a change $\Delta\sigma$ in the total cross section resulting from nuclear orientation is accompanied by a change $\Delta\sigma(0°)$ in the zero-degree elastic cross section, a change $\Delta\alpha$ in the transmission of the holmium sample, and a change $\Delta R$ in the ratio of counts recorded by detectors $D_1$ and $D_2$ in Fig. 7 or Fig. 11. If $(\Delta\sigma/\sigma)$ is small, we may write

$$\frac{\Delta\sigma}{\sigma} = \frac{\Delta\alpha}{\alpha \ln\alpha} \quad \text{(A4)}$$

where

$$\frac{\Delta\alpha}{\alpha} = \frac{\Delta R}{R}(1+\rho_B)\left[1-\rho_{in}\frac{\Delta\sigma(0°)}{\sigma(0°)}\frac{R}{\Delta R}\right],$$
$$\rho_B = (N_B/N_T), \quad \text{(A5)}$$
$$\rho_{in} = \sigma(0°)n_s\left[\frac{d_1+d_2}{d_1 d_2}\right]^2.$$

$N_B$ and $N_T$ are the number of background and transmitted neutrons detected in detector $D_2$, $n_s$ is the total number of nuclei in the holmium sample, and $d_1$ and $d_2$ are the distances from the neutron source and detector $D_2$ to the center of the sample. Eq. (A5) treats the background and inscattering corrections only to first order, and is valid if these corrections are small. The quantity $N_B/N_T$ was measured experimentally; $\sigma(0°)$ and $\Delta\sigma(0°)$ were calculated using the optical parameters given in Figs. 15 and 16.

## APPENDIX IV: ESTIMATE OF $V_{ss}$ FROM A MICROSCOPIC MODEL

The spin-dependent part of the two body $n$-$p$ potential may be written $[V_{0T}(r)-V_{0S}(r)]\boldsymbol{\sigma}_n\cdot\boldsymbol{\sigma}_p$ where $V_{0T}(r)$ and $V_{0S}(r)$ are the triplet and singlet potentials and $\boldsymbol{\sigma}_n$ and $\boldsymbol{\sigma}_p$ are the neutron and proton spin operators. We assume that the ground state of $Ho^{165}$ is described by a single proton bound in a Nilsson orbit about a spin zero core. The principal term in the proton wave function has the quantum numbers[54] $L=5$, $\Lambda=3$, $\Sigma=+\frac{1}{2}$, and for present purposes we will neglect the other components of the proton wave function. $\Sigma$ is the projection of the proton spin on the body-fixed axis. Since $\Sigma=+\frac{1}{2}$, it follows that if $(\mathbf{I}\cdot\boldsymbol{\sigma}_n/I)=1$, $\boldsymbol{\sigma}_n\cdot\boldsymbol{\sigma}_p=1$; i.e., if the spins of the nucleus and the incident neutron are parallel, the spins of the incident neutron and the extra core proton are also parallel and vice-versa. We then assume

$$\int [V_{0T}(r_1)-V_{0S}(r_1)]dV_1 = -\int V_{ss}f(r_2,r_0A^{1/3},a)dV_2.$$

[54] S. G. Nilsson, Kgl. Danske Videnskab. Selskab, Mat.-Fys. Medd. **29**, No. 16 (1955); B. R. Mottelson and S. G. Nilsson, Kgl. Danske Videnskab. Selskab, Mat.-Fys. Skrifter **1**, No. 8 (1959).

TABLE V. Summary of all experimental data on $\Delta\sigma_{\mathrm{Def}}$ and $\Delta\sigma_{\mathrm{ss}}$. $B_1/B_1(\max)$ and $B_2/B_2(\max)$ are the first and second moments of the nuclear orientation and are expressed in a reference frame in which the $z$ axis is parallel to the direction of the neutron beam except in the cases indicated. $P_n$ is the neutron polarization. Where no uncertainties are quoted, none were quoted in the corresponding reference and the uncertainties may be assumed to be negligible. The columns for $\Delta\sigma_{\mathrm{Def}}$ and $\Delta\sigma_{\mathrm{ss}}$ do not include uncertainties in the nuclear orientation parameters.

| $E_n$ (MeV) | $\sigma_T$ (b) | $B_1/B_1(\max)$ | $B_2/B_2(\max)$ | $P_n$ | $\Delta\sigma_{\mathrm{Def}}$ (mb) | $\Delta\sigma_{\mathrm{ss}}$ (mb) | Source |
|---|---|---|---|---|---|---|---|
| 8.0 | 4.97±0.11 | 0.55 ±0.03 | +0.25 ±0.05 | ··· | −38± 10 | | Present exp. |
| 15.0 | 5.27±0.09 | 0.55 ±0.03 | +0.25 ±0.05 | ··· | −139±16 | | Present exp. |
| 0.350 | 7.94 | 0.15[a]±0.03 | +0.54[a,b]±0.04 | ··· | +350±100 | | Ref. 8 |
| 14.0 | 5.29±0.10 | 0 | +0.54[a,b]±0.04 | ··· | +183± 39 | | Ref. 9 |
| 7.85 | 4.97±0.11 | 0.55 ±0.03 | +0.25 ±0.05 | 0.34±0.02 | | +3 ±13 | Present exp. |
| 0.350 | 7.94 | 0.15[a]±0.03 | 0.54[a] ±0.04 | 0.55 | | +30 ±85 | Ref. 8 |
| 0.920 | ··· | 0.31[a]±0.03 | ··· | 0.30±0.03 | | −128[c]±66 | Ref. 49 |

[a] $z$ axis perpendicular to direction of neutron beam.
[b] For purposes of comparison with the present experiment, this orientation may also be described in a reference frame with the $z$ axis parallel to the direction of the neutron beam and $B_2/B_2(\max) = -0.25$.
[c] See, however, Sec. VI B of text.

The integral on the left represents the "integrated strength" of the spin dependent part of the $n$-$p$ potential and, using the values of Hulthén and Sugawara[55] for $V_{0T}(r)$ and $V_{0S}(r)$, is equal to $-\frac{4}{3}\pi(20)$ MeV F$^3$. The integral on the right represents the "integrated strength" of the spin-spin potential and, taking $r_0A^{1/3} = 6.8$ F for Ho$^{165}$, is approximately $-\frac{4}{3}\pi(320)(V_{\mathrm{ss}})$ F$^3$. Therefore, $V_{\mathrm{ss}} \approx +60$ keV. Although this crude estimate might be expected to be good to factor of 2 or 3 at best, it is included to give the reader some feeling for the fact that a small value for $V_{\mathrm{ss}}$ is quite reasonable in the case of Ho$^{165}$.

[55] L. Hulthén and M. Sugawara, in *Handbuch der Physik*, edited by S. Flügge (Springer-Verlag, Berlin, 1957), Vol. 39, p. 1.

# Erratum

**Ground-State Transition Width of the 7.297-MeV Level in $^{208}$Pb,** E. J. DOWDY AND J. A. MCINTYRE [Phys. Rev. **145**, 982 (1966)]. The transition width reported above has been reinvestigated using a different geometry for the beam of 7.297-MeV $\gamma$ rays used to excite a level in $^{208}$Pb. With the new geometry there is no evidence of an excitation in $^{208}$Pb. It is conjectured, therefore, that the 7.297-MeV $\gamma$-ray beam used previously was contaminated in some unknown manner with 7.277-MeV $\gamma$ rays from neutron capture in iron; these $\gamma$ rays are known to excite strongly a level in $^{208}$Pb. Analysis of the absorption measurement reported in this paper using the known energy spread of the iron $\gamma$ rays gives a transition width $\Gamma_0$ for the 7.277-MeV level in $^{208}$Pb having the value of 1.4±0.25 eV. This value is reasonably close to the literature value of 0.8±0.2 eV. We therefore conclude that the excitation reported for the 7.297-MeV nitrogen $\gamma$ ray was spurious; we offer, as an explanation for the resonance excitation found, the excitation of $^{208}$Pb by the 7.277-MeV iron $\gamma$ ray. We acknowledge the contributions of S. Ramchandran and C. J. Kapadia in making the new measurements and calculations.